-

Modelling Network Data Traffic

D.K. Arrowsmith[1], R.J. Mondragón[2]

[1]School of Mathematical Sciences
[2] Department of Electronic Engineering

Queen Mary, University of London

Contents

The aim of these notes is to describe the behaviour of packet traffic flowing on realistic networks as packet load is varied. We are concerned with producing relevant data models for the internet traffic and the statistics - dynamical systems is described first. Specifically, intermittency in iterated maps is used to provide binary data of various types (including em long-range dependent). The dynamical modelling of packet traffic using Erramilli intermittency maps and the dynamics of Transmission Control Protocols is introduced. Regular and scale free network topologies are used to describe Internet packet traffic modelling and the phase transitional behaviour of packet lifetimes on these networks under increasing load. Variation of other features under increasing load are also considered such as transmission and queue capacity.

1 Introduction

These notes are an extended version of the chapter Data Traffic, Topology and Congestion in the book *Complex Dynamics in Communication Networks* [35] and are concerned with the interaction between the topology of a network and the traffic carried along its channels. The binding elements between the topology and the traffic dynamics are the routing mechanisms. In a packet-based network, like the Internet, the transmission of information is done in discrete packets. The path that a packet follows when travelling the network is determined by the routing algorithm. Usually, from the topological properties of the network and statistical properties of the traffic, the routing algorithm tries to minimise the packet delivery time and maximise the throughput; this implies that packet flow affects the behaviour of the routers which in return regulate the flow. The dynamics of a packet network can also be regulated by controlling the packet production at the various packet sources. An example of this control is the *Transmission Control Protocol* or *TCP*, where the source of traffic adjusts its rate of packet transmission as a function of the round trip delay time.

Previously the statistical properties of packet traffic, which are dependent on the control and routing algorithms, were described by a model where the traffic input was *Poisson-like* where the auto-correlation decays exponentially fast. Traffic with this decay property, of which the Poisson type is a particular example, is generically referred to *Short Range Dependence* (*SRD*). From studies carried out in the early 1990's [22] it is known that *Poisson-like* models do not capture all the statistical properties of packet traffic. Packet traffic exhibits spurts of activity over a large number of time scales. These bursts last from milliseconds to days and they look similar independently of the time scale. This phenomenon is known as *self-similar* traffic. One characteristic of this self-similar traffic is that it has *Long Range Dependence* (*LRD*), i.e. the traffic is strongly correlated at all time scales of engineering interest. This observation was a surprise as, previously, the properties of packet traffic were described as *SRD* processes. We start in section 2 by briefly discussing some of the properties of *LRD* packet traffic.

Even though some researchers [31, 50] have suggested that the burstiness in packet traffic is connected to the behaviour of individual users within the network, the modelling of packet traffic

is based on its measured characteristics more than on the underlying mechanisms responsible for the self-similarity. There exist different approaches to describing bursty traffic. These are mainly stochastic methods based on Gaussian self-similar processes, for example fractional Brownian motion and fractional Gaussian noise [45, 39, 40, 60, 30] or, on the superposition of *on/off* sources with *heavy tailed on* or *off* periods [62] and chaotic maps [19, 20, 49]. All these models describe successfully the burstiness of the traffic but their approach is very different. In section 3 we introduce a non-linear chaotic map as a model to generate packet traffic with varying statistical properties. We also discuss several equivalent deterministic models for packet production models which have calculational advantages. The packet production dynamics is also extended to employ the *TCP* window dynamics [18].

The packet delivery time is the time that elapses between the creation of a packet at its source s, to the arrival at its destination d. This time is known as the *end-to-end* time, packet *lifetime* or *latency*. A packet travels through the network visiting different nodes. If one of the nodes is busy, the packet is put in the queue at that node. Eventually, as the node serves its queue, the packet is forwarded toward its destination. Usually longer routes and/or congested queues mean longer delivery times. The routing algorithm tries to reduce the packet delivery time by selecting short, lightly utilised routes. In a lowly utilised network, the traffic characteristics are not drastically changed as the packet transverses the network. The delivery time for a packet from its source to its destination is finite. As the load increases, the delivery time will typically increase accordingly. There is a critical load where the delivery time diverges, or at least increases dramatically. At this point the network is congested.

In a regular-symmetric network, it is possible to predict the traffic load where congestion occurs (a dynamical characteristic) by only considering the average of the shortest path lengths from all sources to all destinations (a topological characteristic) [26, 24, 52, 65]. In section 4 the relevant topological characteristics when studying congestion are introduced and the network dynamics is introduced in section 5.

In section 6 we make the connection between the traffic characteristics, the topology of the network and congestion by looking first at *Poisson* traffic and then at the differences when the input traffic is *LRD*. In section 7 we briefly introduce some mechanisms to control *LRD* traffic, by limiting the size of the queues [65], by reducing the rate of packet production [57] and by using *TCP*-like control [66].

2 Long-Range Dependence

In 1994, *LRD* was shown to be a feature of Internet packet traffic by Leland *et al.*, [37]. The *LRD* behaviour manifests itself along a communication channel as *bursty* activity in the packet rate (no of packets/unit time) which persists on all relevant time scales. The bursty traffic makes it much more difficult to implement effective traffic congestion protocols (e.g. *TCP*).

The statistical nature of *LRD* traffic is formally defined in [10]. A key requirement is that the

autocorrelation of packet traces, $\gamma(k)$, where the lag is k, satisfies a power law decay of the form $\gamma(k) \sim Ck^{-\beta}$, where $\beta \in (0,1)$ and C is constant. Equivalently, $\gamma(k) \sim k^{-2+2H}$, where $H = 1 - \beta/2 \in (\frac{1}{2}, 1)$ is the *Hurst* parameter, [10]. By comparison, *Poisson* traffic has an exponential rate of decay $\gamma(k) \sim C\alpha^{-k}$ with $\alpha > 1$. The Hurst parameter distinguishes between *LRD* traffic for $H \approx 1$ and the *onset* of *SRD* traffic for $H \approx 1/2$, when the autocorrelation decay changes to exponential.

The essential contrast between *SRD*, Poisson-like traffic, arising typically from traditional voice traffic, and the bursty nature of Internet *LRD* traffic is seen in Fig. 1. The effect of scaling is shown for (a) long-range dependent and (b) short-range dependent traffic for a time series of a random variable $X_n, n = 0, 1, 2, \ldots$ The data is averaged in batch sizes of $N = 1$, 10, 100 and $N = 1000$.

The standard deviation in the *Poisson* traffic varies as the square root of the batch size, or magnification, and we see a 'smoothing' of the traffic as N increases in Fig. 1(b). Thus the mean is an increasingly effective indicator of the instantaneous load, i.e expected packet rate, in the traffic. By comparison, for *LRD* traffic, we see that the variation around the mean remains relatively high for large N in Fig. 1(a). Even when averaged over longer time intervals by several orders of magnitude, we still see extreme packet rates which are close to 0 and 1 (cf. Fig. 1(c)). Figure 1(d) shows the power law decay of the autocorrelation function of a *LRD* traffic trace compared with a *SRD* ($H = 0.5$) trace.

One of the consequences of *LRD* traffic is that it increases queue lengths and latency dramatically. The length of a queue fed with *LRD* traffic sources decays as a power law, compared with an exponential decay if it is fed with *Poisson* traffic sources. The effects of *LRD* cannot be 'removed' by a control mechanism and *LRD* needs to be allowed for, both in computer models of network behaviour and in the routing algorithms used to control data flow through networks.

3 Packet production model

Previous simulations of *em SRD* packet traffic generation at each host have used *em SRD* Poisson (or Markovian) distributions. In this case a packet is created at a host only if a random number on the $\mathbb{I} = \{x | x \in [0,1]\}$, interval is below a discriminator value λ. Hence, for a uniform random distribution the average rate at which packets are produced at a host is λ.

An alternative to this is to use chaotic maps to model the *LRD* nature of real packet traffic. We used the family of maps $f = f_{(m_1,m_2,d)} : \mathbb{I} \to \mathbb{I}$ defined in the unit interval $\mathbb{I}$ by $x_{n+1} = f(x_n)$ where

$$x_{n+1} = \begin{cases} x_n + (1-d)\left(\dfrac{x_n}{d}\right)^{m_1}, & x_n \in [0,\, d], \\ \\ x_n + d\left(\dfrac{1-x_n}{1-d}\right)^{m_2}, & x_n \in (d,\, 1], \end{cases} \tag{1}$$

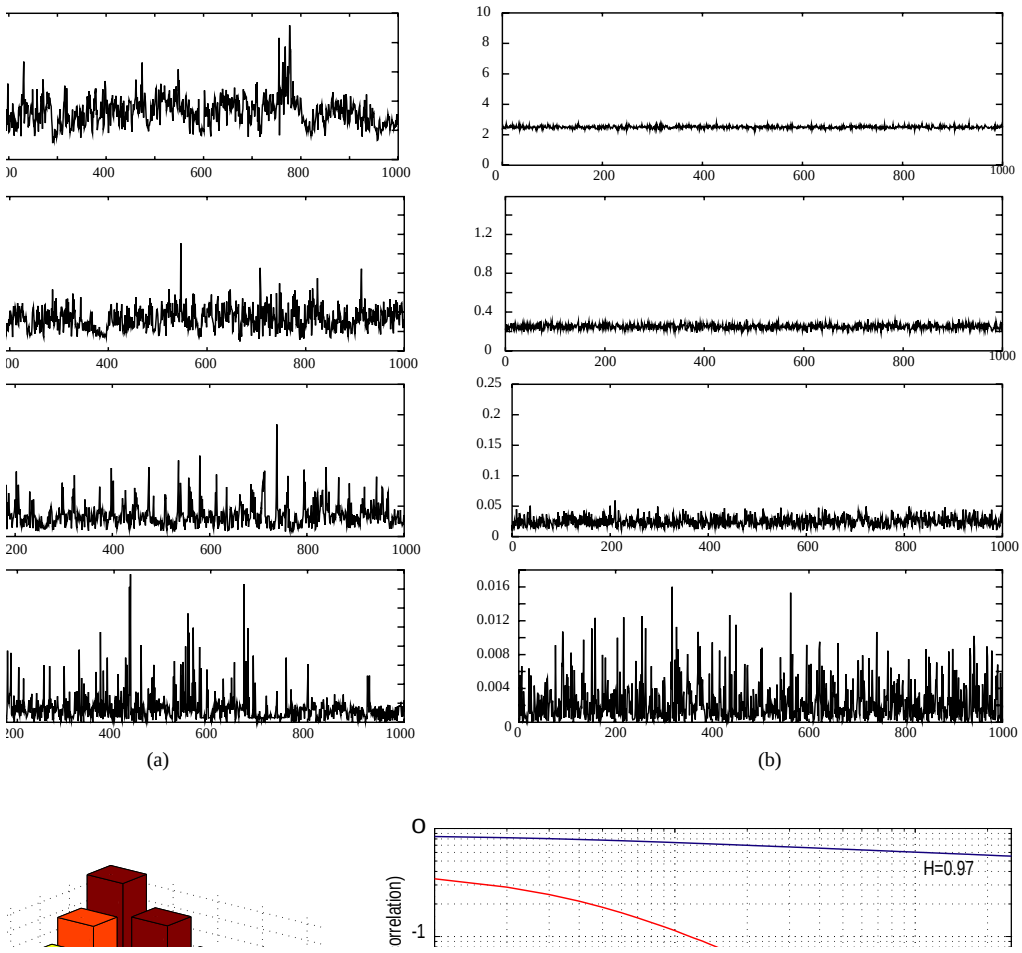

Figure 1: The batch averages of packets/unit time for (a) a real *LRD* traffic trace (Bellcore data from http://ita.ee.lbl.gov/html/contrib/BC.html), and (b) a Poisson based trace for the same load. Each for sizes $N = 1, 10, 100$ and $N = 1000$. A relatively large variance is retained in case (a). (c) Variance for a range of batch sizes and H values. The decay in variance with increasing batch size is much less at the higher H value. For large values of H the mean value can still vary considerably between batches. (d) Autocorrelation function of a *SRD* and a *LRD* traffic trace.

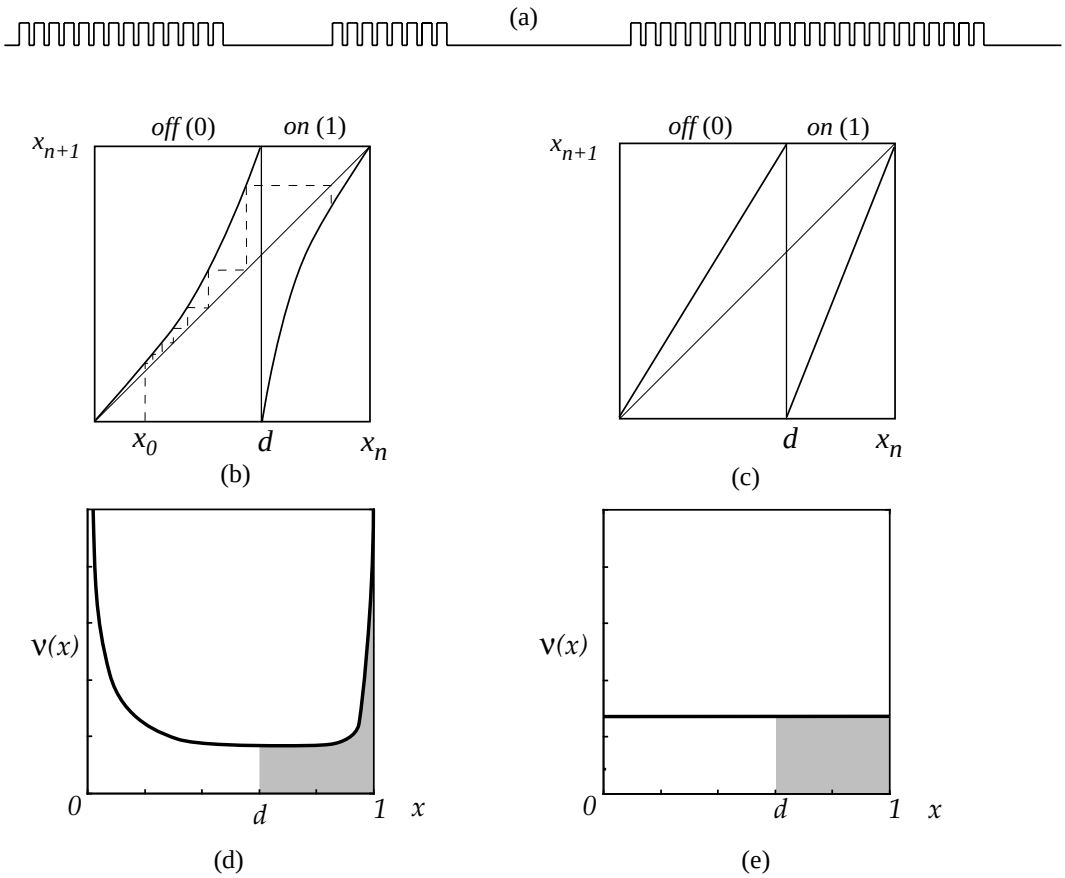

Figure 2: (a) The traffic on a packet network is represented by a binary sequence of zeros and ones (eq. 2). (b) The graph of the map f (eq. 1) consists of two segments and each has a tangency with the line $y = x$. The iteration of the map f with initial condition x_0 forms a 'web' generating the iterative sequence, or orbit, x_n, where $x_n = f(x_{n-1})$, $n = 1, 2, \ldots$. Note that the tangencies at $x = 0, 1$ give a 'slow' change in the values of the sequence x_n, and therefore the output y_n provides long sequences of consecutive '0's or '1's. (c) Graph of f for $m_1 = m_2 = 1$, this is known as the Bernoulli shift map and it generates *Poisson* traffic. If the map parameters are chosen to satisfy $m_1 = m_2 \in \{1, \frac{3}{2}\}$, then the map generates *SRD* traffic.

described in previous papers (see Erramilli *et al*, [19]), and related maps in [51, 61]. Here $d \in (0,1)$ and the parameters m_1, $m_2 \in (\frac{3}{2}, 2)$ induce *intermittency* at each of the points $x = 0$ and $x = 1$, by producing tangencies to the diagonal in the graph of f. The orbital 'escape time' in neighbourhoods of 0 and 1 become power law dependent. If this map is iterated a large number of times, the values of x_n will form a non-uniform continuous distribution on the interval $\mathbb{I}$. The parameter d is used as a discriminator, as λ is for the Poisson case. If x_n falls between 0 and d, a packet is generated; and if x_n falls between d and 1, no packet is generated. Thus we have a discrete output map associated with the function (1) which is

$$y_n = \begin{cases} 1: & x_n \in [0,\, d] \,-\, \text{packet generated}\,, \\ 0: & x_n \in (d,\, 1] \,-\, \text{no packet generated}\,. \end{cases} \tag{2}$$

The above model, which represents the traffic as a binary sequence is also known as a *packet train* model [32] (see Fig. 2(a)). The intermittency behaviour of the map f induces so-called 'memory' in the digital output y_n giving the long range correlation effects required for the packet traffic. This feature is shown by the slow decay of variance with respect to n, the size of batched output, see Fig. 1(a) and [37]. The power-decay of the variance arises from the small orbital increments of the intermittency map which in turn provides memory in the digital output. An example of this phenomenon is illustrated in Fig. 2(b) where a sequence of the iterated values x near the origin have small increments. This effect is even stronger for orbits passing closer to $x = 0$. The time of escape (i.e. into the region $x > d$) of an orbit from a neighbourhood of the origin has a power-law dependence on its initial position, [51].
The nonlinear nature of f means that in this case the load $\lambda = \lambda(m_1,\, m_2,\, d)$ (i.e. the average value of the output y per iteration) is not equal to d, but is given by $\lambda = \int_0^d \nu(x)\, dx$, where ν is the natural invariant density distribution of the map f on the interval $[0, d]$. As an example, Fig. 2(d) shows the shape of the invariant density for the intermittency map. This distribution has no closed form and is often obtained numerically via the Perron-Frobenius operator [41]. Thus the various statistical properties of traffic generated in this way are determined by the map's parameters m_1, m_2 and d including the auto-correlation behaviour as we shall see in section 3.1.4.

3.1 Equivalent packet production models

3.1.1 Closed form map

There are two other important models which have useful mathematical characteristics not available in the standard model described above. The first extension was introduced by Pruthi [48], and the closed form model appears, at first sight, to be more intractable than the original model

in equation (1). Essentially, the function in (1) is replaced by

$$x_{n+1} = \begin{cases} \dfrac{x_n}{(1 - c_1 x_n^{m_1 - 1})^{\frac{1}{m_1 - 1}}}, & x_n \in [0,\, d], \\ \\ 1 - \dfrac{1 - x_n}{(1 - c_2 (1 - x_n)^{m_2 - 1})^{\frac{1}{m_2 - 1}}}, & x_n \in (d,\, 1], \end{cases} \tag{3}$$

where

$$c_1 = \frac{1 - d^{m_1 - 1}}{d^{m_1 - 1}}, \qquad c_2 = \frac{1 - (1 - d)^{m_2 - 1}}{(1 - d)^{m_2 - 1}}. \tag{4}$$

A Taylor expansion gives the form of the equation (1) and so the leading intermittency effects are the same in both models with leading exponents m_1 and m_2. A distinct advantage of (3) is that, somewhat remarkably, it has a closed form under composition. If the first branch function is denoted by $f_1(c_1,\, m_1,\, x)$ then the n-th iterate can be shown to satisfy $f_1^n(c_1,\, m_1,\, x) = f_1(nc_1,\, m_1,\, x)$. Similarly the second branch function f_2 satisfies $f_2^n(c_2,\, m_2,\, x) = f_2(nc_2,\, m_2,\, x)$. This enables sojourn times in the "*off*" or "*on*" regions to be calculated explicitly, by solving equations of the type $f_1^n(c_1,\, m_1,\, x) = d$, to obtain the number of iterations to the transition point. This map will be used in subsection 3.3 and also in the subsection 3.1.3 to obtain a simple derivation of escape time.

3.1.2 Piece-wise linear map

A second model which has different mathematical advantages over the original Erramilli model is a piece-wise version. This was originally introduced by Wang [61] and has been used subsequently in applications to realise maps with given autocorrelation profiles [9]. The analogue is constructed with the use of two sequences. The piecewise linear maps $p : \mathbb{I} \to \mathbb{I}$ are defined by two monotonic sequences z_i^L and z_i^R monotonic decreasing to zero, with $z_1^L = z_1^R = 0.5$. The graph of the map is piecewise linear with nodal points defined by $(z_i^L,\, z_{i+1}^L)$, and $(1 - z_{i+1}^R,\, 1 - z_i^R)$, $i = 1, 2, \ldots$. The piecewise linear map can replicate the intermittency behaviour at $x = 0, 1$ by choosing the sequences to decay to zero in an appropriate way. If we let $z_i^L \sim i^{-\alpha}$ and $z_i^R \sim i^{-\beta}$ with $\alpha, \beta > 1$, then the exponents for the different types of smooth and piecewise linear map have analogous asymptotic behaviour at the intermittency points. We identify the parameters as $\alpha = 1 + 1/m_1$, and $\beta = 1 + 1/m_2$. The piece-wise linear map has distinct advantages in that it is possible to calculate the invariant measure associated with the map, see [9].

3.1.3 Power-law escape

We can use the closed iterative form above to calculate the probability of 'escape' from an intermittency region. Specifically, we consider the probability of a sequence of k-consecutive

zeroes for the output y_n of an intermittency map f. We will use the closed form map

$$f(x) = \frac{x}{(1 - c_1 x^{m-1})^{\frac{1}{m-1}}} \tag{5}$$

for $0 \leq x \leq d$ and will assume a random uniform injection into the region $[0, d]$ for $x > d$, see [47].
If the orbit re-enters the interval $[0, d]$ at the point $\bar{x}$, then that determines the sequence length l of zeroes, namely,

$$l(\bar{x}) = \frac{1}{c_1}\left(\frac{1}{\bar{x}^{m-1}} - \frac{1}{d^{m-1}}\right) \tag{6}$$

Let $P(l(x))$ be the probability density for at least length l "zero" sequences. If we are assuming that the initial point density on the interval $[0, d]$ at $\{\bar{x}\}$ is $\hat{P}(\bar{x})$

$$\hat{P}(\bar{x})d\bar{x} = P(l(\bar{x}))dl. \tag{7}$$

If we further assume the re-entry density $\hat{P}(\bar{x})$ to be uniformly random, i.e. a constant, then

$$P(l) = \left|\frac{d\bar{x}}{dl}\right| \sim Cl^{-\frac{m}{m-1}} \tag{8}$$

for small x with C a constant. This is not the case for re-entry to the interval $[0, d]$ when the full double intermittency is used.

3.1.4 Autocorrelation of the map output

The average $E(G)$ of the function $G(x)$ with respect to an orbit $\{x_i\}_{i=1}^{\infty}$ is

$$\begin{aligned} E(G) &= \lim_{N\to\infty} \frac{1}{N}\sum_{i=1}^{N} G(x_i) = \lim_{N\to\infty} \frac{1}{N}\sum_{i=1}^{N} \int G(x)\delta(x - x_i)\, dx \\ &= \int G(x) \lim_{N\to\infty} \frac{1}{N}\sum_{i=1}^{N} \delta(x - x_i)\, dx \\ &= \int G(x)\nu(x)\, dx. \end{aligned} \tag{9}$$

We have already seen in Fig. 1 that the movement between strings of the output values '0' and '1' is rapid in trace (b) and much slower in trace (a). The intermittency in traffic maps produces increased sojourn times for the two states. The longer sojourn times are said to introduce *memory* into the output which is reflected in a higher correlation between the output binary sequence and the same sequence with a time-lag k. The *autocorrelation* vector of a sequence is

the way in which the memory is measured. Let X_t be a scalar time series of the binary values $\{0, 1\}$ for $t = 0, 1, 2, \ldots$, and suppose the series is stationary. We define the autocorrelation of time lag k by

$$\gamma(k) = \frac{E(X_t X_{t+k}) - E(X_t)E(X_{t+k})}{\sqrt{(\mathrm{Var}(X_t)\mathrm{Var}(X_{t+k}))}}. \tag{10}$$

Let $\mu = E(X_t)$. Note that the values X_t are binary, then $E(X_t^2) = E(X_t) = \mu$ and so $\mathrm{Var}(X_t) = E(X_t^2) - E(X_t)^2 = \mu(1-\mu)$. Therefore, the autocorrelation can be re-written

$$\gamma(k) = \frac{E(X_t X_{t+k}) - \mu^2}{\mu(1-\mu)} \tag{11}$$

Given $0 \leq X_t X_{t+k} \leq X_t$, it follows that $\gamma(k) \leq 1$. Note also that if there is no correlation, i.e. the values X_t are independent of each other, then $E(X_t X_{t+k}) = E(X_t)E(X_{t+k})$ and $\gamma(k) = 0$. Thus, in general, we expect that the correlation coefficient $\gamma(k)$ will eventually decay to zero in some way. Two special types of decay are

(a) power-law decay, where $\gamma(k) \sim Ck^{-\beta}$, for some constant C and $\beta > 0$;

(b) exponential decay, where $\gamma(k) \sim C\alpha^{-k}$, for some constants C and $\alpha > 0$.

For comparison, consider the correlation behaviour of the piece-wise linear Bernoulli map $f(x) = 2x \bmod 1$ on the interval [0, 1]. Given the current state is '0', then $0 \leq x < 0.5$. The probability of the transfer '$0 \to 0$' is 0.5, since it requires $0 \leq x < 0.25$, and similarly for '$1 \to 1$'. Thus we can calculate exactly

$$Pr('1 \to 1') = 0.25 \tag{12}$$

within one iteration, as it is one of four possible binary pairings all equally likely. For correlations over $k > 1$ iterations of the orbit $\{X_n\}$, we have

$$Pr(x_{t+k} = 1, x_t = 1) = Pr(x_t = 1)Pr(x_{t+k} = 1 | x_t = 1) = 0.5^2 = 0.25 \tag{13}$$

and hence $E(X_t X_{t+k}) = 0.25$. The uniform density in the interval $\mathbb{I}$ gives $E(X) = 0.5$. The time series X_t is binary and so $X_t^2 = X_t$, which implies $E(X^2) = E(X)$. It follows that $\mathrm{Var}(X) = E(X^2) - E(X)^2 = E(X) - E(X)^2 = 0.5 - 0.5^2 = 0.25$. Therefore

$$\gamma(k) = \begin{cases} 1 & \text{for } k = 0 \\ (0.25 - 0.5^2)/0.25 = 0 & \text{for } k > 0. \end{cases} \tag{14}$$

The instant correlation decay for the doubling map should be compared with the power law decay in equation (8).

3.2 Autocorrelation for intermittency maps

Only two exact results are known so far for the asymptotic properties of double intermittency maps considered here. If we consider the piecewise linear maps constructed from two sequences $z_i = i^{-\alpha}$ at $x = 0$ and $w_i = 1 - i^{-\alpha}$ at $x = 1$, α, $\beta > 1$, then the two intermittencies compete and it can be shown that

$$\gamma(k) \sim K\, k^{-c} \tag{15}$$

where $c = \min\{\alpha, \beta\} - 1$, K constant, [9]. Thus the correlation for the composite map is determined by the heaviest tail in the correlation decay arising from the two competing intermittencies.

A similar result is also available for the differentiable case [43]. In this case, the map is as in eqn. (1) with the extra condition that whenever f iterates across the line $x = d$, the formula is replaced by a random uniform injection. For example, the autocorrelation vector $c(n), n \in \mathbb{Z}^+$, of the output function y is known to have asymptotic behaviour $\gamma(n) \sim n^{-\beta}$ up to a multiplicative constant, as $n \to \infty$ with $\beta = (2 - m)/(m - 1) \in (0, 1)$ for $m = \max\{m_1, m_2\}$ with m_1, $m_2 \in (\frac{3}{2}, 2)$, [27, 43, 9]. Furthermore, the Hurst parameter, H, is given by

$$H = 1 - \frac{\beta}{2} = \frac{3m - 4}{2(m - 1)}, \tag{16}$$

and ranges over the interval $(\frac{1}{2}, 1)$, as required. Thus m_1, $m_2 = 1.5$ corresponds to Poisson-like behaviour and as m_1, m_2 are increased towards 2, the behaviour is increasingly long-range dependent, see [9, 43]. Fig. 2(c) shows the shape of the *SRD* map obtained when $m_1 = m_2 = 1.0$ and (e) its invariant density. If the transition simplification is removed then the result that the heaviest tail dominates in the piece-wise smooth case is still open but the auto-correlation decay is conjectured to remain as in eqn (16).

3.3 Transmission Control Protocol Dynamics

The dynamics of the packet production model can be extended to incorporate packet window dynamics [18]. If the map is in the '*on*' state, each iteration of the map represents a packet generated. One sojourn period in the '*on*' side of the map represents a whole file. These *files* are then *windowed* using the *slow-start* algorithm, adding another dynamical layer to the system. The algorithm is as follows:

At a given host i in the network, and time $t = n$, there is a current state, $x_i(n)$, and a current window size, $w_i(n)$, for the number of packets that can be sent at time $t = n$. There is also a residual file size, $s_i(n)$, at node i which is given by the number of iterates of f such that $f^{s_i(n)}(x_i(n)) < d$, and $f^{s_i(n)+1}(x_i(n)) > d$. The source will send $p_i(n) = \min\{w_i(n), s_i(n)\}$ packets. The full dynamics therefore takes the form, (see Erramilli *et al.*, [18]):

For $x(n) < d$, i.e. packet generated-

$$w_i(n+1) = \begin{cases} 1, & \text{if } x_i(n-1) < d, \\ \min\{2w_i(n),\, w_{max}\}, & \text{otherwise,} \end{cases} \tag{17}$$

and $x_i(n+1) = f^{p_i(n)}(x_i(n))$.
For $x_i(n) > d$, i.e. no packet generated - $w_i(n+1) = 0$, and $x_i(n+1) = f(x_i(n))$.
This algorithm applies if all packets in a window are acknowledged before the retransmission timeout (RTO) limit is reached. If packets take longer than this to be acknowledged the window of packets is sent again with the RTO doubled and the window size set to zero. When the map is '*off*' the window size is zero and no packets are sent.
This initial value of RTO is calculated using the exponential averaging method [53]. This method keeps a running average of all round trip times. This average is weighted towards more recent round trips, and is used in calculating the initial RTO.

4 Topology of Networks

Many different topologies appear in communication networks. Square lattices, toroidal lattices, meshes and hypercubes arise on multiprocessor computers (e.g. [38]), scale-free networks in the WWW [4] and the Internet [21, 42]. The way that the elements of the network are connected to each other and the nodal degree properties have an impact on its functionality. The representation and study of the connectivity of a network is carried out using concepts from graph theory.
A communications network can be represented by a graph $\mathcal{G} = (\mathcal{V}, \mathcal{E})$, where $\mathcal{V}$ is the set of nodes (vertices) and $\mathcal{E}$ is the set of links (edges). The hosts, routers and switches are represented by nodes and the physical connections between them are represented by links. The links can have a direction, but here we are only going to consider undirected links. A node can transfer information to another node in the form of data-packets if there is a link between them. If there is no direct link between the nodes, then a path in the network is the sequence of distinct nodes visited when transferring data-packets from one node to another. We consider networks where there exists at least one path connecting any pair of nodes of the network.
The degree, k, of a node is the number of links which have the node as an end-point [63], or equivalently, the number of nearest neighbours of a node (see Fig. 3(a)). The degree of a node is a local quantity. However, the node degree distribution of the entire network gives important information about the global properties of a network and can be used to characterise different network topologies.
If there is very little traffic on the network and if the journey time from one node to its neighbour is in unit time, then given any two nodes and to first approximation, the journey time will be proportional to the length of the journey, or the path length. A path that goes from source node

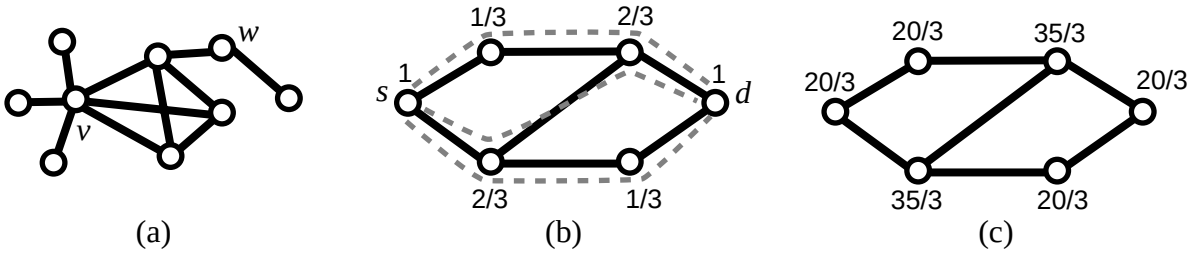

Figure 3: (a) The node degree for node v is 6 and for w, it is 2. (b) Three different shortest paths between s and d. The length of the path is 3. The number above the nodes denotes the proportion of shortest paths $p_{s,d}(w)$ that go through that node. (c) The node medial centrality for the whole network.

s, to destination node d, in the smallest number of hops is called the shortest-path. The length of the shortest-path $\ell_{s,d}$ is the number of nodes visited when going from s to d. There can be more than one shortest–path between a pair of nodes. The characteristic path length

$$\bar{\ell} = \frac{1}{S(S-1)} \sum_{s \in \mathcal{V}} \sum_{d \neq s \in \mathcal{V}} \ell_{s,d}, \tag{18}$$

where S is the total number of nodes, is the average shortest-path over all pairs of nodes (see Fig. 3(b)). Sometimes $\bar{\ell}$ is referred to as the diameter of the network.

If there is traffic on the network the difference in the journey times of two shortest paths with the same length can be very different. Not all the journeys are equal due to the different patterns of usage of the routes. On a network, there are nodes that are more prominent because they are highly used when transferring packet-data. A way to measure this "importance" is by using the concept of *betweeness centrality* of a node. The concept of centrality [23] was introduced in social networks to characterise the prominence of an individual in the *context of the social structure*. Given a source s, and destination d, the number of different shortest-paths is $g(s,d)$. The number of shortest-paths that contain the node w is $g(w;s,d)$. The proportion of shortest-paths, from s to d, which contain node w is

$$p_{s,d}(w) = \frac{g(w;s,d)}{g(s,d)}. \tag{19}$$

Remark: The proportion of shortest-paths and the shortest-path length are related by

$$\ell_{s,d} = \sum_{w \in \mathcal{W}} p_{s,d}(w) - 1, \tag{20}$$

where $\mathcal{W}$ is the set that contains the nodes visited by the shortest paths from s to d.

The *betweeness centrality* of node w is defined as [29]

$$\mathcal{C}_B(w) = \sum_{s \in \mathcal{V}} \sum_{d \neq s \in \mathcal{V}} p_{s,d}(w) \tag{21}$$

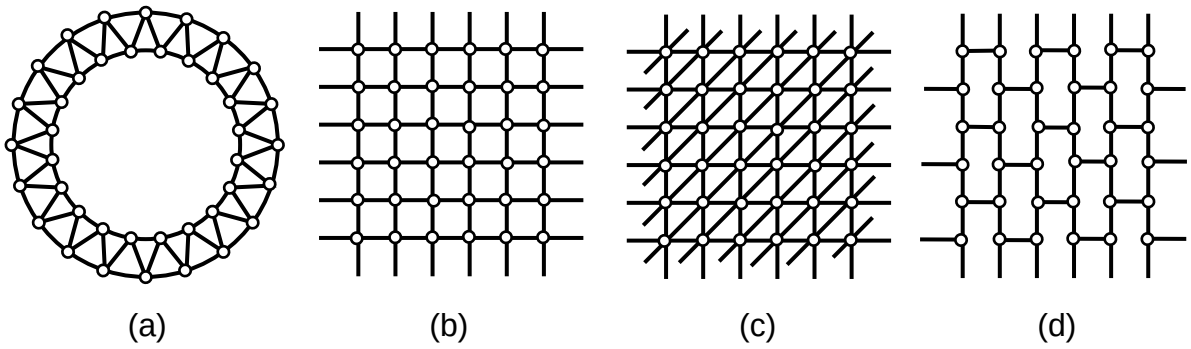

Figure 4: Four regular-symmetric networks. (a) The ring network and (b) the rectangular toroidal network, in which the nodes on one edge of the lattice connect to nodes on the opposite edge, have degree four. (c) The triangular toroidal network has degree six and (d) the hexagonal toroidal network has degree three.

where the sum is over all possible pairs of nodes with $s \neq d$. The betweeness centrality measures how many shortest paths pass a certain node (see Fig. 3(c)) A node with a large $\mathcal{C}_B$ is "important" because a large amount of packets flow through it, that is, it carries a large traffic load. If this node fails or gets congested, the consequences to the network traffic can be very drastic [29, 69].

4.1 Regular-Symmetric Networks

In a regular network all nodes have the same degree (see Fig. 4). By symmetry, the betweeness centrality is constant for all nodes. From Eq. (20) and if $\mathcal{C}_B(w) = c$ then

$$c = \frac{1}{S} \sum_{w \in \mathcal{V}} \mathcal{C}_B(w) = \frac{1}{S} \sum_{s,d} \ell_{s,d} - 1. \tag{22}$$

4.1.1 Toroidal networks [52, 24, 46, 65]

The toroidal rectangular network ($\mathcal{H}$) is based on a square lattice of nodes in which each node has four neighbours with boundary nodes appropriately identified. The finite rectangular lattice $\mathbb{Z}$ consists of $S = L^2$ nodes. The position of each node in the lattice is given by the coordinate vector $\mathbf{r} = (i, j)$ where i and j are integers in the range 1 to L. The network has periodic boundary conditions throughout, and so each coordinate of (i, j) is effectively reduced - mod $L + 1$ to give a toroidal topology. To measure the distance between a pair of nodes the periodic "Manhattan" metric

$$d_{pm}(\mathbf{r}_1, \mathbf{r}_2) = L - \left| |i_2 - i_1| - \frac{L}{2} \right| - \left| |j_2 - j_1| - \frac{L}{2} \right| \tag{23}$$

is used, where the points $\mathbf{r}_1 = (i_1, j_1)$ and $\mathbf{r}_2 = (i_2, j_2)$ of $\mathbb{Z}$ give the positions of the two nodes.

The average shortest path is

$$\begin{aligned}\bar{\ell} &= \frac{1}{L^4}\sum_{\mathbf{r}_1,\mathbf{r}_2} d_{pm} = \frac{1}{L^4}\sum_{i_1,i_2,j_1,j_2=1}^{L-1}\left(L - \left|i_2 - i_1| - \frac{L}{2}\right| - \left||j_2 - j_1| - \frac{L}{2}\right|\right) \\ &= \frac{L}{2} \end{aligned} \tag{24}$$

Useful comparative networks for traffic studies are the hexagonal and triangular networks (see Figure 4 (c & d)). Their embeddings in the plane show how we can view the three regular networks as satisfying an edge inclusion property $E(\mathcal{H}) \subset E(\mathcal{R}) \subset E(\mathcal{T})$. Comparative studies of all three types of network show consistent results [65] on the critical loads, and the onset of congestion behaviour.

4.1.2 Planar networks

These are similar to the above toroidal networks but with free boundary conditions. In this case, the Manhattan metric becomes

$$d_m(\mathbf{r}_1, \mathbf{r}_2) = |i_2 - i_1| + |j_2 - j_1|\,. \tag{25}$$

This is not a regular network because the border nodes have less links than the nodes "inside" the network. The average shortest path is

$$\bar{\ell} = \frac{1}{L^4}\sum_{\mathbf{r}_1,\mathbf{r}_2} d_m(\mathbf{r}_1, \mathbf{r}_2) = \frac{2}{3}\frac{L^2 - 1}{L} \approx \frac{2}{3}L \tag{26}$$

4.2 Random Networks

Random networks have been used to model communications networks. The reason is that because some of the communication networks tend to have a complex topology and the interactions defining their structure are apparently random.

Starting from a set of nodes, a random network is built by connecting every pair of nodes with probability p. If the total number of nodes is S and if $p > 1/S$ [12] then the network is fully connected with probability 1, or equivalently, there is at least one path connecting any pair of nodes with probability 1. This is the only case we are going to consider here, as we are interested in connected networks.

The degree distribution of a random graph is well approximated by a binomial distribution [12]

$$P(k) = \binom{S-1}{k} p^k (1-p)^{S-1-k}. \tag{27}$$

The degree distribution tends to be concentrated around some "typical" node degree, or average node degree $\bar{k}$ [17, 11], see Fig. 5. The characteristic path length scales with the size of the

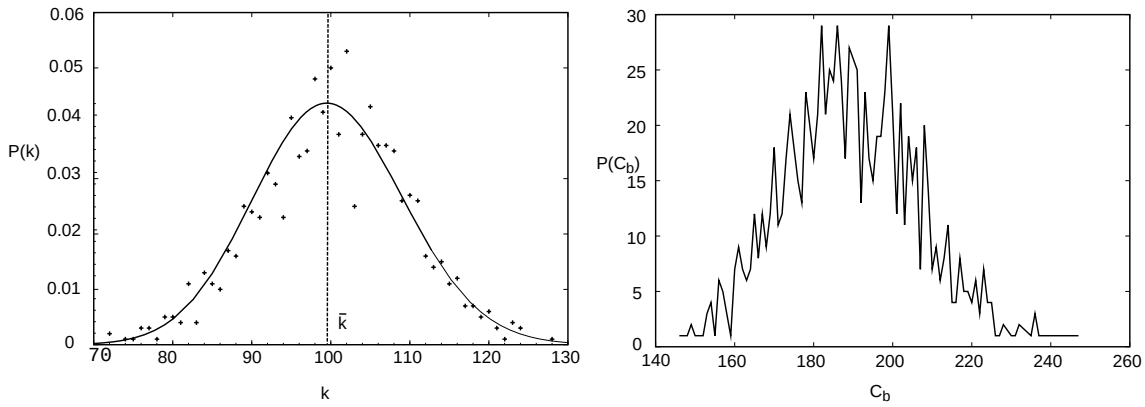

Figure 5: (a) Node degree distribution for a random network with $S = 1000$ and $p = 0.1$, and its approximation using the binomial distribution. (b) Betweenness centrality distribution of the network.

network as

$$\bar{\ell}_{\text{rand}} \approx \frac{\ln(S)}{\ln(\bar{k})} \tag{28}$$

and, of course, this implies that the distance between a pair of nodes is very small compared to the size of the network.

4.3 Scale-free Networks

Many technological networks are not described by a random or a regular network; instead they are better described by a network where the degree distribution is a power law [4, 21]where

$$P(k) \sim Ck^{-\beta}, \tag{29}$$

for $\beta > 1$ and C constant. The probability that a node has k edges connected to it is given by $P(k)$. In practical terms a power law distribution means that the majority of the nodes will have very few neighbours, but there is a very small set of the nodes with a very large number of neighbours (see Fig. 6 (a)). Networks with this property are known as *scale-free* because power-laws are free of a characteristic scale, that is, there is no characteristic node degree (see Fig. 6(b)).

The diameter of a scale-free network scales as $\bar{\ell} \sim \ln\ln S$ [13] where S is the size of the network. This is due to the existence of "far–reaching" links which are shortcuts when going from a source to a destination. Any node that contains one of these far-reaching links is going to be highly used when transferring packet-data, that is, its betweeness centrality is large (see Fig. 6(d)). Fig. 6(b)-(d) shows some properties of the Internet at the domain level, which is a scale-free network.

In 1999, Barabási and Albert [8] showed that it is possible to create a scale-free network by using two generic mechanisms: *growth*, the network grows by attaching a new node with m links to

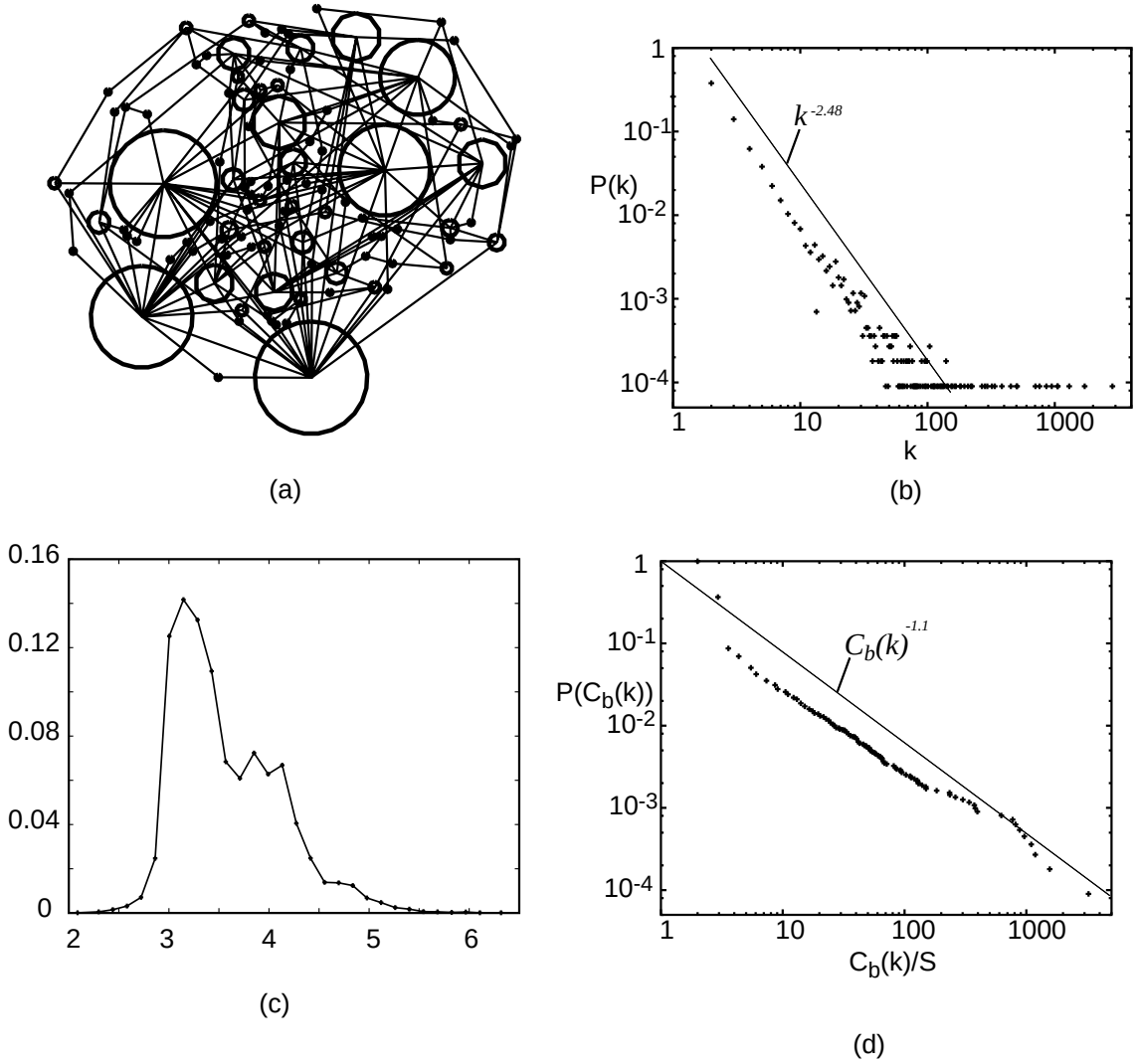

Figure 6: (a) A scale-free network where the size of the node is proportional to its *betweeness centrality*. In this case is clear that there is a correlation between the node degree and its betweeness centrality [28]. (b) Degree distribution $P(k)$ vs. node-degree k, (c) shortest-path length distribution and (d) betweeness centrality for the Internet at the domain level (AS-level). The size of the AS-level Internet is $S = 11,\,122$ and the average path length is 3.13.

m different nodes present in the network; and *preferential attachment*, where new nodes are attached preferentially to nodes that are already well connected. Barabasi and Albert showed further that if the probability that a new node will be connected to node i with degree k_i is

$$\Pi(i) = \frac{k_i}{\sum_j k_j}. \tag{30}$$

then the network has a power law link distribution $P(k) \propto k^{-3}$.

4.3.1 The Internet

In 1999, an analysis of the Internet topology by Faloutsos *et. al* [21] suggested that the distribution of node degrees of the Internet decays as a power-law $P(k) \propto k^{-y}$, with $y = 2.22$. In 2002, Subramanian *et. al* [55] reported that the Internet features a tier structure, where at the top of this tier is the core of the network. It is well established that a realistic model of the Internet topology should generate a power law topology with a core structure. There exist network models that produce power law networks, e.g. Barabási and Albert model [8] and Inet-3.0 [64] to mention just two of them, but they do not reproduce the core structure of the Internet [68]. A node of a network is considered "rich" if it contains a large number of links or equivalently it has a large node-degree. The core of the Internet consist of a set of nodes which have a large node degree. We refer to these nodes as the *rich-club*. In the Internet, the members of the rich-club are very well connected to each other. This means that there are a large number of alternative routing paths between the club members where the average path length inside the club is very small (1 to 2 hops). The rich-club acts as a super traffic hub and provides a large selection of shortcuts. Hence scale-free models without the rich-club structure may underestimate the efficiency and flexibility of the traffic routing in the Internet. Conversely, networks without the rich-club may over-estimate the robustness of the network to a node attack, [3, 29] where the removal of a small percentage of its richest club members can break down the network integrity. It is possible to build network topology models which will generate a rich club. Recently the Interactive-Growth (IG) model [67] was introduced as a way to generate networks that contain a rich-club. The model is a modification of the Barabási and Albert model and it reflects the evolution of the Internet, with the addition of new nodes and the addition of new links between existing nodes. The network is generated by starting with m_0 nodes connected through $m_0 - 1$ links. At each time–step, one of the following two operations is performed: 1) with probability $p \in (0, 1)$, $m < m_0$ new links are added between m pairs of nodes chosen from the existing nodes, and, 2) with probability $1 - p$, one new node is added and connected to m existing nodes, see Fig. 7.

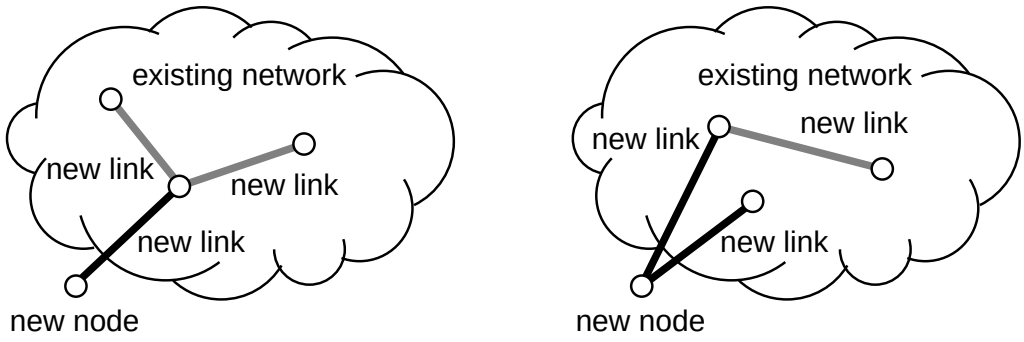

Figure 7: The growth of new nodes and new links are interdependent in the *IG* model. (a) A new node connects to a host and this host creates two new connections to existing nodes. (b) A new node connects to two old nodes and one of the old nodes connects to another old node.

5 Model of Networked Data Traffic

The model considered here has been studied by several authors [46, 24, 26, 25, 52, 57, 65, 5, 7]. The network consists of two types of nodes; router nodes that store and forward packets; host nodes that store and forward packets and are also sources and sinks of traffic. Given the network has S nodes, and a density $\rho \in [0, 1]$ of hosts then ρS is the number of total hosts. The host nodes are randomly distributed in the network.

- Traffic generation: A host creates a packet whose destination is another host. A host creates a packet using either a uniform random distribution (Poisson) or a *LRD* distribution defined by a chaotic map. Each source generates its traffic independently of the other sources.

- Queue: Each node keeps a queue of unlimited length where the packets are stored. Any packet that is generated is put at the end of the host's queue. If a packet arrives at a router it is put at the end of the hierarchical router's queue. The packet is not queued when it arrives at its destination node.

- Routing: Each node picks a packet at the head of the queue and forwards the packet to the next node. From the source/destination information that each packet carries, the forwarding is done by one of the following routing algorithms:

  1. For regular networks:
     - a neighbour closest to the destination node is selected
     - if more than one neighbour is at the minimum distance from the destination, the link to which the smallest number of packets has been forwarded is selected
     - if more than one of these link shares the same minimum number of packets forwarded then a random selection is used
  2. for general networks:

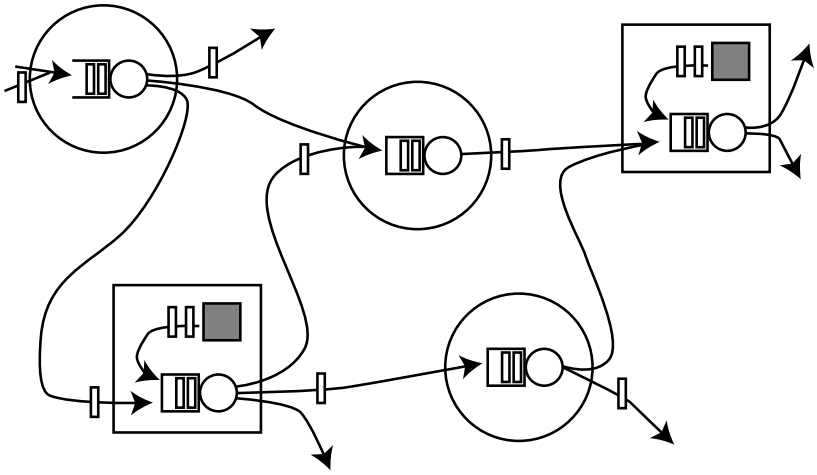

Figure 8: The hosts, represented by large squares, are sources and sinks of traffic. The traffic source is represented by a small gray rectangle. The routers, large circles, only route traffic. Both hosts and routers have a queue where traffic can be stored during its transit through the network.

- From the state of the queues and the number of hops from source to destination, the routing is done by minimising the time–delay by considering the number of hops and the size of the queues that a packet visits when crossing the network.

The process of packet generation, hop movement, queue movement and updating of the routing table occurs at one time step (see figure 8).

6 Congestion

The time that elapses between the creation of a packet at source s, from its creation to its destination d, is known as the delay time $\tau_{s,d}$. The average of the delay

$$\bar{\tau} = \frac{1}{S(S-1)} \sum_{s,d;\tau_{s,d} \leq T} \tau_{s,d},$$

which is the average for all the packets up to time T, is an important quantity with which to assess the performance of a network. If the traffic load presented to the network is low and the queues on the nodes are empty, then, to a first approximation, the average delay is proportional to the average number of nodes that the packets visit when travelling. As the traffic load increases, the queues at the nodes start to build up, the average delay time will increase accordingly. If the traffic load increases even further, then at the critical load λ_c, the queues of some nodes will grow very quickly and the average delay time will dramatically increase or even diverge. At this critical load, we consider that the network is congested. This critical behaviour is also noticed in the network throughput. The throughput is defined as the

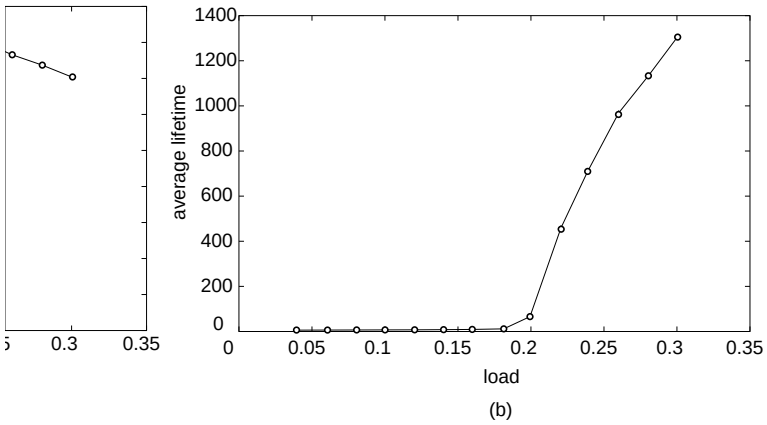

Figure 9: (a) Average throughput of a Manhattan network with $S = 100$ and $\rho = 1$. As the offered load increases the average throughput increase until it reaches the critical point $\lambda_c \approx 0.2$. At this point the network is congested. (b) The average lifetime of a packet increases rapidly after the congestion point.

number of packets reaching their destination per unit time per host. Starting from a low load, the throughput increases proportionally as the increase of the load, until congestion is reached. At this point the network has its maximum throughput (see Fig. 9).

If the number of packets at node i at time t is denoted by $n_i(t)$, then the total number of packets in the network is

$$N(t) = \sum_{i=1}^{S} n_i(t) \leq \sum_{i=1}^{S} Q_i(t), \tag{31}$$

where $Q_i(t)$ is the buffer size of node i. If the network is not congested, and the average delay time is finite, then the average number of packets on the network, $\bar{N} = \lim_{t\to\infty} N(t)/t$, is finite. At the congestion point, the queues of the congested nodes increases rapidly and this implies that the total number of packets on the network continues to increase.

6.1 Mean Field Approximation

6.1.1 Total distance formulation [65]

A simple way of estimating λ_c is to look for the total distance that all the packets at time t have to travel to reach their destination. In the congested phase if there are queues at all nodes, then the change in total distance is $D(N_{t+1}) - D(N_t)$, where $N(t)$ is the number of packets in the queues at time t, and $D(N_t)$ is the aggregated distance of all packets from their destination at time t. The increase in the number of packets per unit of time is $\rho\lambda S$. If $\bar{\ell}$ is the average path length, then the overall added distance is $\rho\lambda S\bar{\ell}$. By contrast, the aggregated distance is reduced by S given that every packet at the head of the queue moves one step closer to its destination.

Thus the change in total distance to destination between time t and $t+1$ is

$$D(N_{t+1}) - D(N_t) = \rho\lambda\bar{\ell}S - S. \tag{32}$$

The critical load λ_c occurs when the total distance no longer decreases, $D(N_{t+1}) - D(N_t) = 0$, which implies

$$\lambda_c = \frac{1}{\rho\bar{\ell}}. \tag{33}$$

This relation refines the results of [52] and [24].

6.1.2 Average Utilisation Model

The above model can be developed further by taking into account the different behaviour for hosts and routers. Given that hosts also route packets, if o_r is the average utilisation of any node queue due only to cross traffic, then the total node utilisation across the whole network can be given by:

$$N = (o_r + \lambda)n_h + o_r n_r \tag{34}$$

where n_h is the number of hosts and n_r is the number of routers. The local critical load condition is given by

$$o_r + \lambda = 1 \tag{35}$$

which implies that the hosts are fully loaded, but the routers are not.
As before, the overall added distance per time step is $\rho\lambda S\bar{\ell}$. Thus the change in total distance to destination between time t and $t+1$ is

$$D(N_{t+1}) - D(N_t) = \rho\lambda\bar{\ell}S - ((o_r\lambda)n_h + o_r n_r). \tag{36}$$

When the total distance no longer decreases we obtain the following equation for o_r:

$$o_r = \rho\lambda(\bar{\ell} - 1). \tag{37}$$

If the average utilization of the queues exceeds the rate at which packets are served, then queues will become overloaded. Since routers handle cross traffic exclusively, the average occupancy of router queues is given simply by o_r. For host queues the packets produced by the source have to be added, so the average occupancy is $o_r + \lambda$. For this network packets are always served at the rate of one per time tick. Thus, if either value exceeds 1 then queues will become overloaded. Substituting the condition for host queues becoming overloaded, $o_r + \lambda = 1$, into Eq. (37) gives the following expression for λ_c' the load at which (local) congestion starts:

$$\lambda_c' = \frac{1}{\rho\bar{\ell} - \rho + 1}. \tag{38}$$

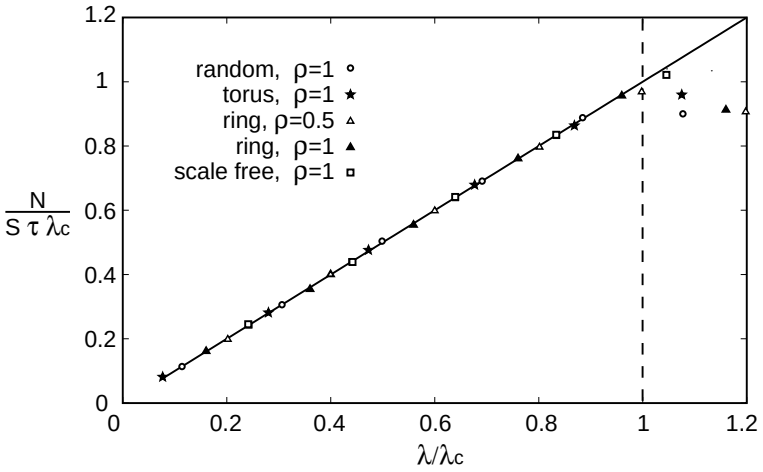

Figure 10: Verification of Little's law for different networks. In all cases the networks have $S = 100$ nodes. The coordinates have been normalised by dividing them by the critical load of the corresponding network. For the ring network, the law was verified for two different densities of nodes. The law does not hold if the load is greater than the critical load (marked with a vertical hash line).

Congestion is present for loads between λ_c' and λ_c. In this case, host queues are overloaded when $o_r + \lambda > 1$, and the congestion spreads to router queues. However, the router queues are not fully utilised until the global criterion is met at $\lambda = \lambda_c$, when the total service capacity of the network is fully matched by the overall added distance of incoming traffic.

6.2 Time-delayed formulation

Another possible way to determine the critical load is to use Little's law [25, 52]: *"The average number of customers in a queueing system is equal to the average arrival rate of customers to that system, times the average time spent in the system"* [34]. Little's law is a flow conservation law which can be restated as: in a steady state, the number of delivered packets is equal to the number of generated packets, or

$$\frac{d\,N(t)}{d\,t} = \rho\lambda S - \frac{N(t)}{\tau(t)}. \tag{39}$$

where $\rho\lambda S$ is the average arrival rate to the queues per unit of time, $\tau(t)$ is the average time spent in the system, and $N(t)/\tau(t)$ is the number of packets delivered per unit of time.
Remark: Little's law does not depend on the arrival distribution of packets to the queue or the service time distribution of the queues. Also it does not depend upon the number of queues in the system or upon the queueing discipline within the system. The law holds only when a steady state exists below the critical load, as shown in Fig. 10 where the load rates have been normalised.
If the load is low, the queues at the nodes tend to be empty and the average delay time is the average shortest path $\bar{\ell}$, that is $\tau \approx \bar{\ell}$. For higher loads the transit time can be approximated

by the average shortest path plus the average time, $\mathcal{T}$, that a packet spends in the queues

$$\tau \approx \bar{\ell} + \mathcal{T}(N(t), \bar{\ell}). \tag{40}$$

6.2.1 Criticality for Regular-Symmetric Networks

If the traffic is evenly distributed in the network and the network is not congested, then there exists a steady state solution N^* for the number of packets on the network. Each queue, on average, contains N^*/S packets and the delay can be approximated by

$$\tau(t) \approx \bar{\ell}\left(1 + \bar{Q}\right) = \bar{\ell}\left(1 + \frac{N^*}{S}\right) \tag{41}$$

where on average, a packet visits $\bar{\ell}$ queues with average load $\bar{Q}$ and $\mathcal{T} \approx \bar{\ell}\bar{Q}$. From the steady state solution ($d\,N(t)/d\,t = 0$) the total number of packets in the system is

$$N^* = \frac{\rho\lambda\bar{\ell}S}{1 - \rho\lambda\bar{\ell}} = \frac{\gamma S}{1 - \gamma} \tag{42}$$

where $\gamma = \rho\lambda\bar{\ell}$ is the normalised load and N^* is the steady state solution.
The average traffic load generated at node i is

$$\lambda_i = \left(\frac{1}{\rho\bar{\ell}(1 + S/N^*)}\right). \tag{43}$$

As the traffic load increases, the number of packets in the network increases accordingly. At the congestion point the number of packets on the network diverges, $N^* \to \infty$, and the critical load is

$$\lambda_c = \frac{1}{\rho\bar{\ell}}, \tag{44}$$

which is the same as Eq. (33).

6.2.2 General networks

Fig. 11 shows, in phase space, that the transition from the free flow phase to the congested phase is well approximated by Eq. (44) for the case of regular-symmetric networks but not for scale-free networks. Equation (44) gives a good approximation to the critical load because the average queue size for all nodes is very similar ($\bar{Q} \approx N^*/S$).
In a scale-free network, due to the disproportionate importance of some of the nodes, if these nodes get congested more readily and hence, all the network gets congested. An alternative approach is to use the betweeness centrality [44] to characterise the node usage. If

$$\hat{\mathcal{C}}_B(w) = \frac{\mathcal{C}_B(w)}{\sum_{v\in\mathcal{V}} \mathcal{C}_B(v)} \tag{45}$$

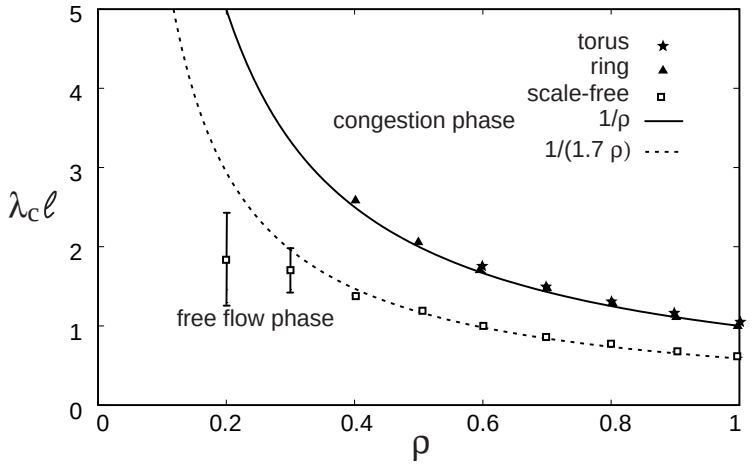

Figure 11: Phase diagram showing the change from free–flow to congestion. For the square toroidal and the regular-symmetric network the phase transition is given by $\ell_c \lambda_c = 1/\rho$. For $\rho > 0.4$ the phase transition of the scale free network is well approximated by $\ell_c \lambda_c = 1/(1.7\rho)$.

is the normalised betweeness centrality then the average queue size at node i can be approximated by

$$\bar{Q}_i \approx \hat{\mathcal{C}}_B(n_i) N^*. \tag{46}$$

An example of this approximation is shown in Fig. 12.
It is possible to approximate the typical travel time of a packet by adding the average time that the packets spends in the queues that it visits, that is

$$\tau^*(s,d) \approx \sum_{v \in \mathcal{R}(s,d)} \hat{\mathcal{C}}_B(v) N^* \tag{47}$$

where the sum is over all nodes that the packet visits. The set $\mathcal{R}(s,d)$ is the subset of nodes obtained from the routing table. The total delay time can be approximated by considering

$$\tau(t) \approx \bar{\ell} + \frac{1}{S(S-1)} \sum_{s \in \mathcal{V}} \sum_{d \neq s \in \mathcal{V}} \sum_{v \in \mathcal{R}(s,d)} \hat{\mathcal{C}}_B(v)\, N(t) = \bar{\ell} + \mathcal{D} N(t) \tag{48}$$

where

$$\mathcal{D} = \frac{1}{S(S-1)} \sum_{s \in \mathcal{V}} \sum_{d \neq s \in \mathcal{V}} \sum_{v \in \mathcal{R}(s,d)} \hat{\mathcal{C}}_B(v). \tag{49}$$

The approximation to the critical load is given by

$$\lambda_c = \frac{1}{\rho S \mathcal{D}}, \tag{50}$$

(cf. Eq. (44)). As shown in Fig. 13, this last equation gives a very good approximation of the phase transition from free flow phase to congested phase for the regular-symmetric and scale-free networks.

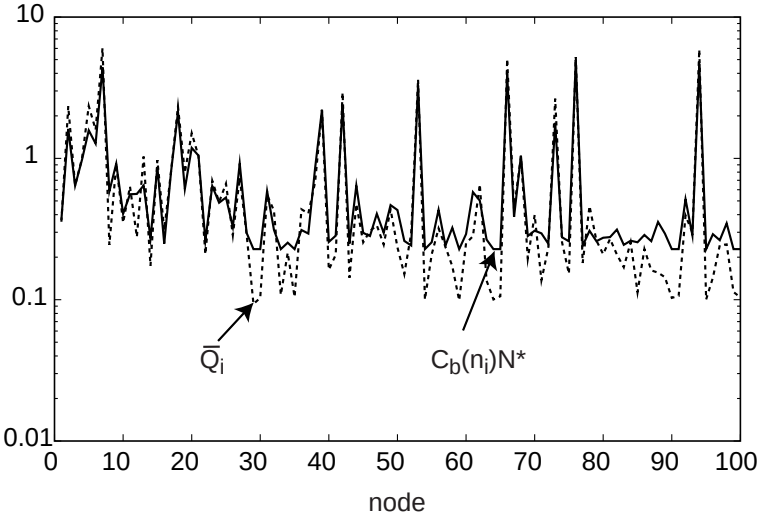

Figure 12: Comparison between the average queue size (dotted line) and its approximation using Eq. (46) (solid line). The network is a scale-free network with $S = 100$.

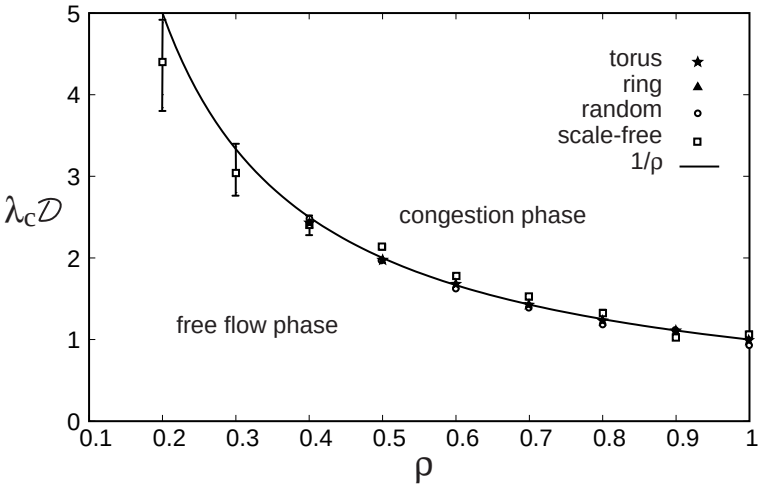

Figure 13: Renormalised phase transition for different networks topologies. The four networks have $S = 100$.

It is not difficult to see why Eq. (50) also works for regular-symmetric networks. If the betweeness centrality measures how many routes use a particular node, then all nodes are utilised to the same degree in the regular case. The constant value for the betweeness centrality for each node is the same (see Eq. (22)) and is given by

$$\hat{\mathcal{C}}_B(w) = \frac{\mathcal{C}_B(w)}{\sum_{v\in\mathcal{V}} \mathcal{C}_B(v)} = \frac{1}{S}. \tag{51}$$

Then

$$\begin{aligned} \frac{1}{S(S-1)} \sum_{s\in\mathcal{V}} \sum_{d\neq s\in\mathcal{V}} \sum_{v\in\mathcal{R}(s,d)} \hat{\mathcal{C}}_B(v) &= \frac{1}{S(S-1)} \sum_{s\in\mathcal{V}} \sum_{d\neq s\in\mathcal{V}} \sum_{v\in\mathcal{R}(s,d)} \frac{1}{S} \\ &= \frac{1}{S(S-1)} \sum_{s\in\mathcal{V}} \sum_{d\neq s\in\mathcal{V}} \frac{\ell_{s,d}}{S} = \frac{\bar{\ell}}{S}. \end{aligned} \tag{52}$$

By substituting this last expression in Eq. (50) the expression for the critical load obtained in Eq. (44) is recovered.

Equation (50) also reproduces the following behaviour observed by Fks and Lawniczak [24] in a rectangular network. The addition of a small number of random links, in a rectangular network, reduces the value of the critical load in spite of the increased connectivity between the nodes, see Fig. 14. The addition of some random links provides a shortcut between distant parts of the network. Since the packets are forwarded to their destinations via the shortest path, it often happens that one link serves as a shortcut for many packets in a neighbourhood. In some respect the additional links "attract" a large part of the traffic and quickly get congested. From the figure, it is clear that the use of betweeness centrality reflects this increase in the node usage and, hence, its importance when evaluating the onset of congestion.

6.2.3 *LRD* at criticality

It is known that at the critical load the traffic statistics change from *SRD* to *LRD* [52]. The change of correlations from *SRD* (exponential) to *LRD* (power law) at criticality in phase transitions is a standard feature, and this phenomena also occurs in road traffic congestion.

The change from *Poisson* to *LRD* can be observed by analysing the time series for delays for 1 hop and 24 hop routes, and also by looking at the time series of average host and router queues lengths measured at each time tick. As mentioned before, the Hurst parameter distinguishes *SRD* traffic from *LRD*. The parameter can be obtained by considering the so-called *rescaled data*. More precisely, let X_t, $t \in \mathbb{Z}^+$ denote a discrete time series. The *adjusted range* is defined as

$$R(t,k) = \max_{0\leq i\leq k} R_i(t,k) - \min_{0\leq i\leq k} R_i(t,k), \tag{53}$$

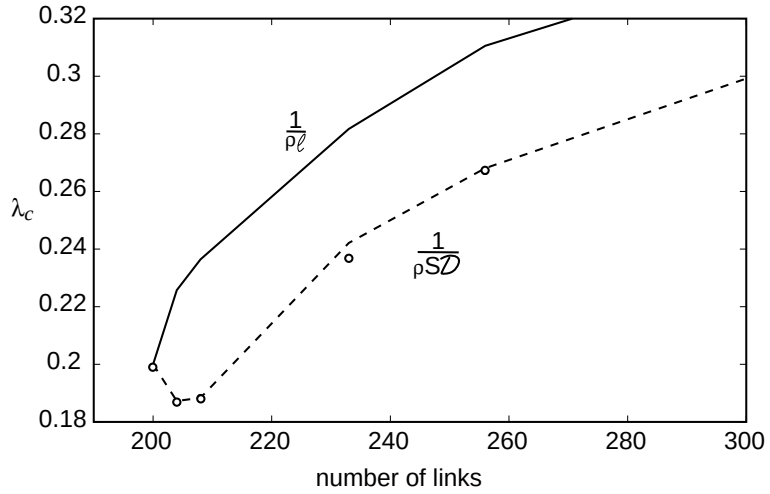

Figure 14: Decrease of the critical load due to the addition of random links in a rectangular network with $S = 100$ and 200 bidirectional links. The solid line is the value of the critical load obtained using Eq. (44). The dashed line is the critical load obtained from Eq. (50). The circles are the values of the critical load obtained from the numerical experiment.

where

$$R_i(t,k) = \sum_{l=1}^{t+i} X_l - \sum_{l=1}^{t} X_l - \frac{i}{k}\left(\sum_{l=t+1}^{t+k} X_l - \sum_{l=1}^{t} X_l\right) \tag{54}$$

The quantity $R(t,k)$ is normalized by the translated sample standard deviation

$$S(t,k) = \sqrt{k^{-1}\sum_{l=t+1}^{t+k}(X_l - \bar{X}_{t,k})^2} \tag{55}$$

where $\bar{X}_{t,k} = k^{-1}\sum_{l=t+1}^{t+k} X_l$. The R/S statistic is then defined to be

$$R/S_t(k) = \frac{R(t,k)}{S(t,k)} \tag{56}$$

and it is fitted to the equation

$$\ln E[R/S(k)] = a + H \ln k, \tag{57}$$

with H interpreted as the Hurst parameter. In Table I we consider separate R/S plots for 1 and 24 step journeys in a 32×32 network grid with 164 hosts for Poisson, and for LRD sources for a range of load values. The network used had the same parameters as that used for Fig. 15 so the onset of congestion at a load of 0.3 was expected. At the smaller loads the network remains free of congestion. This means that time series of packet delays are stationary, and the original data may be used in measuring a value of H. For the higher values of the load, including

Table 1. Hurst H-values for Poisson sources.

Load λ	$l = 1$	$l = 24$
0.2	0.51	0.57
0.29	0.71	0.70
0.30	0.54	0.53
0.39	0.52	0.51
0.45	0.56	0.57

$\lambda = 0.3$, congestion does occur, leading to an upward trend in delay times and queue sizes. In this case, the data are weighted to remove the trend, creating a stationary series. In Table I Poisson we see that for $\lambda = 0.2$, $H = 0.5$ for both path lengths, indicating that very little *LRD* is present. This is corroborated by investigating the probability distributions of delays which both have the characteristic shape of exponentially decaying delay times. However, for $\lambda = 0.29$ H values are higher for both path lengths. The R/S plots show a kink with the steeper part of the curve corresponding to $H = 0.8$ in both cases. Hence the longer delays and lower frequencies do show significant *LRD*, but this is not seen at any other load value. Values for the three higher load values show very similar H values. Note that in these cases, the time series was weighted to remove the upward trend and the H values are all close to 0.5. This lack of any *LRD* seems to be caused by the phase change to the congested region above λ_c'. The probability distributions for these higher values show delays shifting towards the length of the run (1×10^6 time ticks as the network becomes more and more congested. Here 1 and 24 step delays have a long tailed distribution, but this is caused by the non-stationarity of the data, not power-law autocorrelation decay.

6.2.4 Congestion and *LRD* traffic

In the previous section, it was noted that *LRD* arose from interaction within the network and was not intrinsic to the traffic sources. In this section the Poisson-like sources are replaced with *LRD* sources, modelled using chaotic maps.

Fig. 15 gives a comparison of the onset of congestion in two otherwise identical networks with host density $\rho = 0.164$, one Poisson sourced, and the other *LRD* sourced for different values of the Hurst parameter. The values of the intermittency parameters $m_1 = m_2 = m$ are kept equal in each case for simplicity. The critical load for this network is $\lambda = 0.3$.

Fig. 15(a) shows the average lifetime, or *end-to-end delay*, of a packet plotted against load λ, the average number of packets generated per host per unit time. As has been seen previously, there is a phase transition from the free phase in which lifetimes remain small to a congested phase in which lifetimes increase rapidly. Fig. 15(a) shows clear evidence of the earlier onset of congestion in the *LRD* traffic in comparison with Poisson traffic produced at the same rate. The data for Fig. 15 are shown for various values of $m_1 = m_2$. Values of $m_1 = m_2$ close to the maximum value of $m_1 = m_2 = 2$ give the highest degree of intermittency and hence the greatest

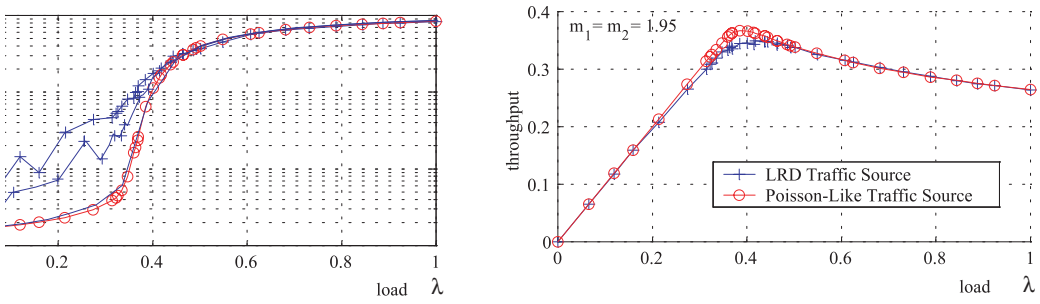

Figure 15: (a) Average packet lifetimes are plotted as a function of the load λ for Poisson sources and also for *LRD* sources with increasing average lifetime in the pre-congestion phase as m increases through $m_1 = m_2 = 1.5, 1.8$, and 1.95. (b) Corresponding throughput for Poisson and *LRD* traffic are plotted as a function of the load λ for $m = 1.95$. Note that the lower peak value in throughput for the *LRD* traffic sources reflects the longer average lifetimes below the critical point. The peak differences diminish to zero as m is decreased to the Poisson-like value $m = 1.5$.

contrast with Poisson traffic sources (corresponding to $m_1 = m_2 = 1.0$ in the intermittency model). The highest value used in our simulations, $H = 0.975$ has been observed in statistical investigations of real network traffic data.

Fig. 15(b) shows throughput versus load. The peak in the throughput occurs at the critical point. The network therefore reaches its peak efficiency at the critical point. The peak throughput is slightly lower for the *LRD* sources, emphasising the longer lifetimes of packets. Although the throughput is only slightly reduced, the average lifetimes increase by up to a factor of 10. This earlier onset appears to be the most important feature of *LRD* congestion within the context of the model, and has significant implications for shared backbone data network infrastructures.

The average queue sizes are closely related to the average lifetime. Fig. 6.2.4 shows the difference in the average queue size for a rectangular network with *Poisson* and *LRD* traffic. Clearly in the *LRD* case the queues get congested more readily and as mentioned before this translates into longer lifetimes of the packets.

In Table 2 high values of H for queue length distributions at hosts and routers are measured at all post critical loads for Poisson sources indicating the presence of strong network-induced *LRD*.

Table 2. R/S behaviour for time series of (a) average host; (b) average router queue lengths.

	H -	(Poisson)	H -	(*LRD*)
load(λ)	hosts	routers	hosts	routers
0.2	0.69	0.69	1.0	0.95
0.29	0.96	0.78	1.0	1.0
0.3	0.98	0.89	1.0	1.0
0.39	0.99	1.0	0.99	1.0
0.45	0.98	1.0	1.0	1.0

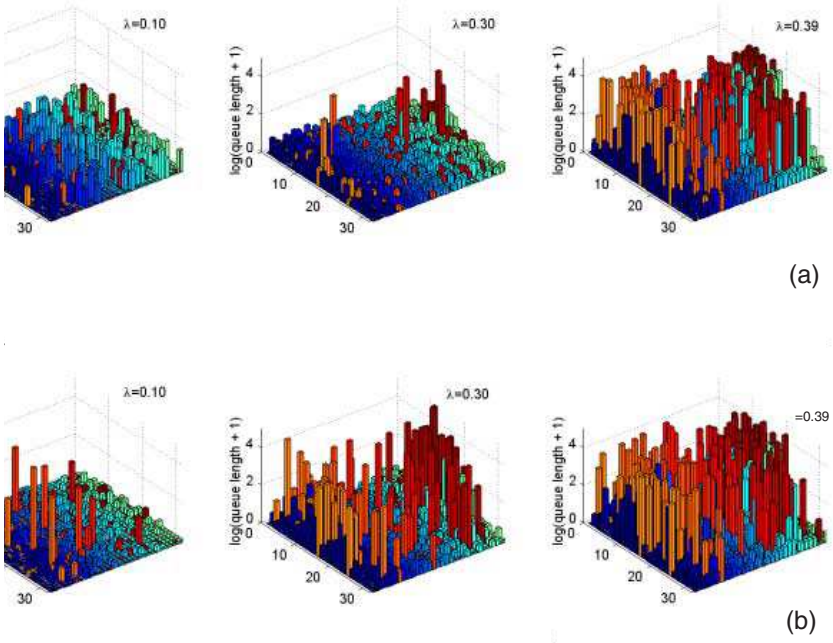

Figure 16: The distribution of queue lengths in a rectangular grid for (a) *Poisson* sources, and (b) *LRD* sources, with pre-critical, critical and congested loads set at the same three values for each type of source. The longer lengths of queues for the *LRD* traffic can be clearly seen.

7 Control

7.1 Control of queue sizes

The simplest way to control packet traffic is to limit the length of queues [6]. As grid bar charts of node queue size have shown by Woolf *et al.* [66], long queues in the network invariably occur at hosts. For this reason it was decided to reduce the rate of packet production at hosts with long queues. The simulation keeps count of packets produced, so the actual or *carried* load is known. Knowledge of the d value being used for the map f gives the maximum rate of packet production, or "offered" load.

Figs 1.17(a) and 1.17(b) show average lifetime and throughput plotted against the carried load. The data apply to a 32×32 node rectangular network with a host density 0.16 and Poisson-like traffic sources. A comparison is made between simulations with and without a queue limit. There is little difference between the two cases below a carried load of $\lambda = 0.3$. Average lifetime and throughput are very similar.

Average queue lengths are closely linked to average lifetime. As has been shown previously, this is the point at which congestion sets in. Above this point average lifetimes and host queue lengths are much lower in the controlled case. In the case of host queue length this would be expected, because when packets are created at a host they are immediately added to the queue for that host. The queue limit device prevents longer queues from building up. This also explains the longer average lifetimes. Long host queues no longer exist, so host packets are not delayed so long and average latency times are therefore lower. The average router queue length is longer in the controlled case because there is no limit on router queue lengths, so that packets that would have been in host queues become distributed over router queues instead. The effect on throughput is much smaller, but there is a slight increase when control is used. It should be noted that the plots extend beyond a carried load of about $\lambda = 0.36$, which is the maximum load with queue limiting. In a real network this would equate to bandwidth being traded or a reduced end-to-end delay.

Figs 1.17(c) and 1.17(d) show similar plots for the same network with *LRD* sources. In this case the average lifetime is very much lower in the controlled case for the whole range of carried load values. As before, the average queue lengths are linked closely to average lifetime. We have seen in the last section that, in the case of *LRD* sources, congestion starts at very low values of load. The queue limiting prevents this early onset of congestion, modifying the system to behave as the same network with Poisson sources would. This can be seen in the plots of average lifetime. Again, higher queue thresholds have less influence. The throughput is slightly higher in the controlled case at high values of the load. As before, the highest possible load when control is used is about $\lambda = 0.36$.

Figs 1.17(a) and 1.17(b) show plots of the same parameters for the same network with Poisson sources, but plotted against carried load instead of offered load. The plot of average lifetime versus offered load shows that in the controlled case average lifetimes remain low even when they

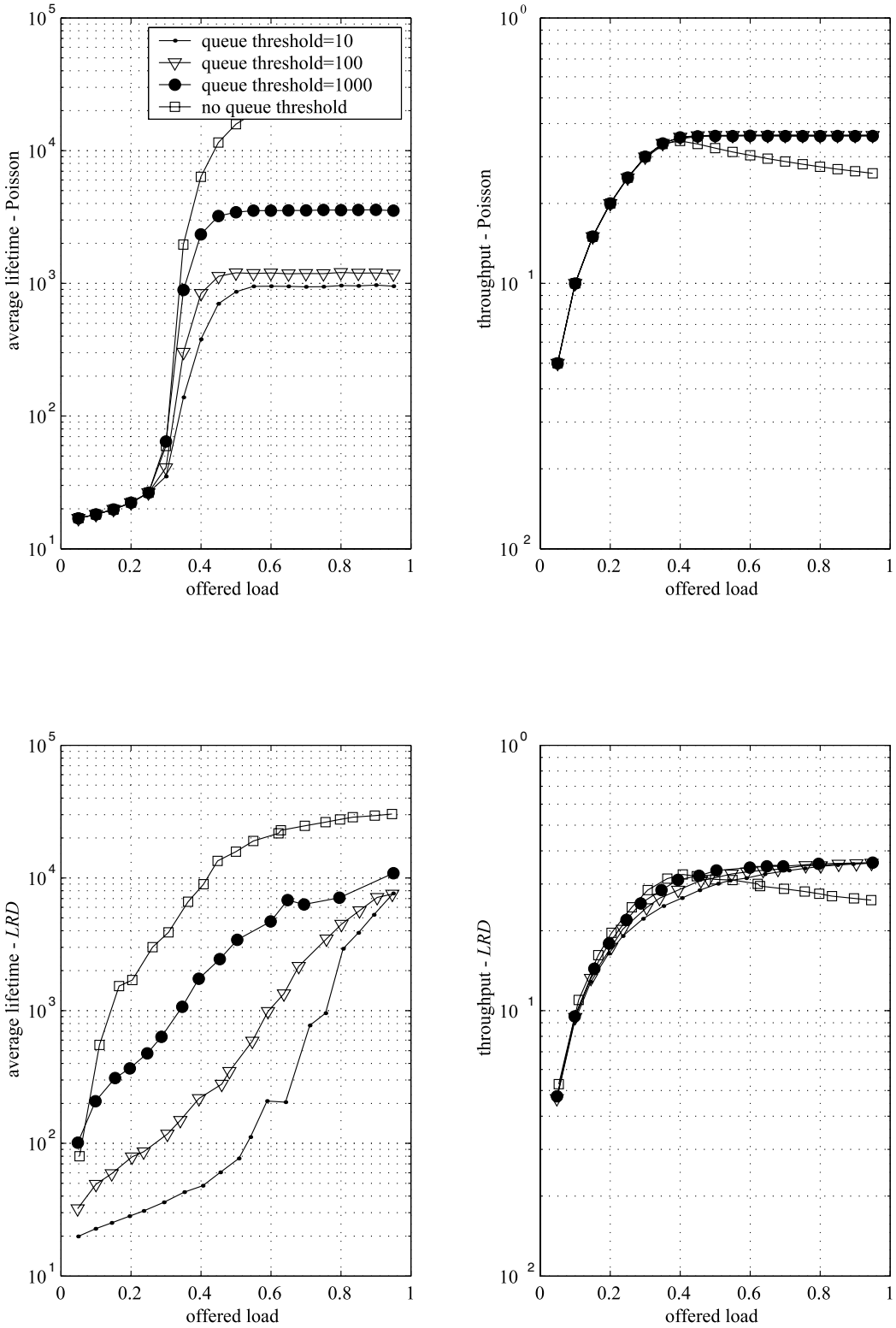

Figure 17: Plots showing the behaviour of the network parameters average lifetime and throughput as offered load is varied when control is applied to a network containing either all Poisson or all *LRD* sources. The network has $S = 164$

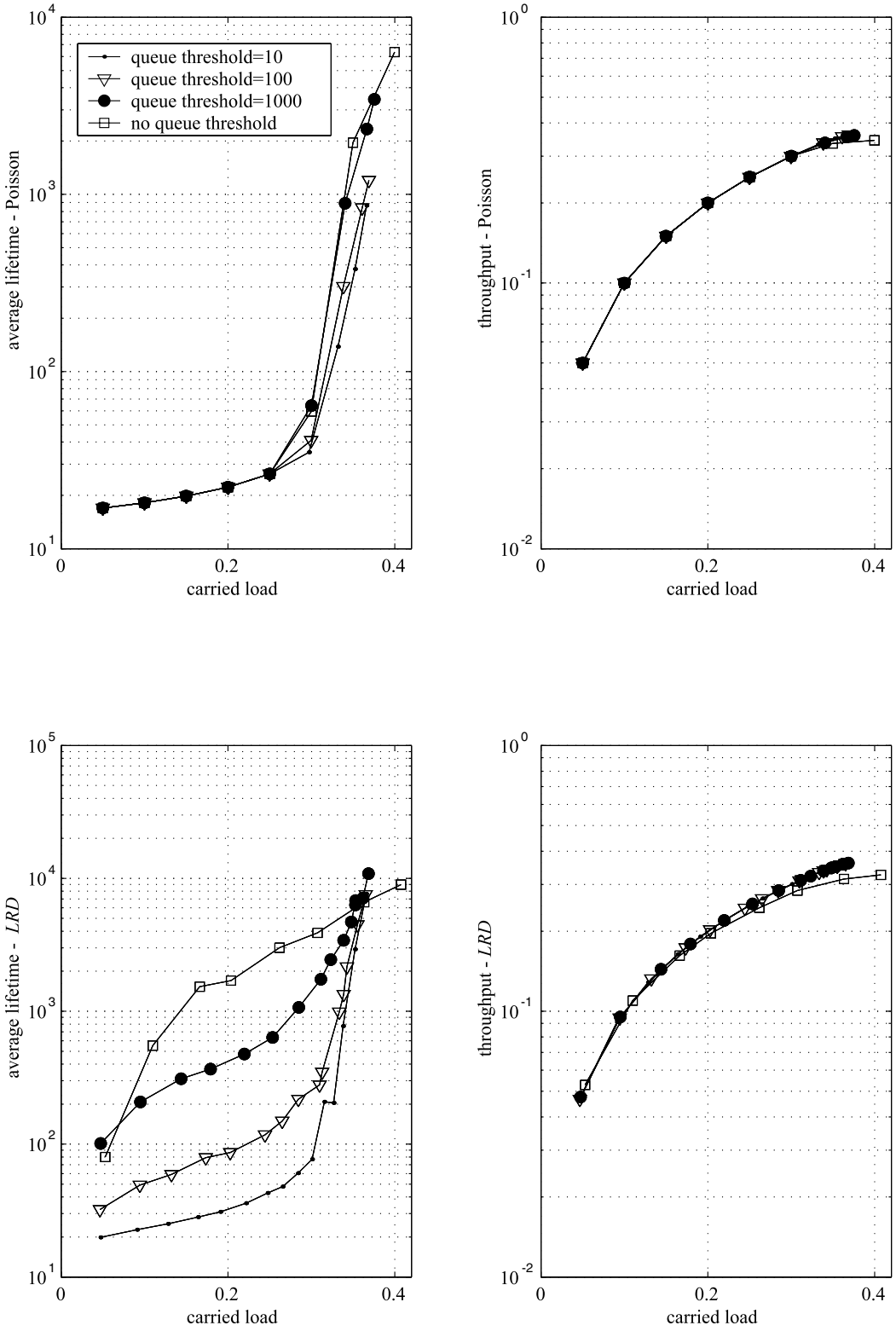

Figure 18: Same as the previous figure but with carried load instead of offered load

would become very high in the uncontrolled case. The same applies to average host queue sizes. In effect, the control mechanism prevents the network from becoming congested, no matter how high the offered load, but at the expense of restricting the carried load to one that the network can manage. Similar conclusions can be drawn for *LRD* sources as shown in Figs 1.18(c) and 1.18(d).

7.2 A local control mechanism and critical behaviour

When a critical load is reached, the deterioration in delivery is fast and wide-reaching. It has already been noted that a key indicator of the onset of congestion is load. At the critical regime, the distribution of duration length scales as a power law, [59, 24]. Valverde and Solé [57] introduced a control mechanism where hosts modify their rates of packet release depending on the detected *local* rate of congestion.

Consider our simplest model with queues of uniform length. Clearly the host sites (those that are either source and destination end-points) must have a controlled injection of packets to ensure a non-overloaded network. As before only a fraction ρ, $(0 < \rho < 1)$ are hosts. The remainder are routers which can only store and transmit the packets. Both hosts and routers can transmit only one packet at a time. The sources adjust their local packet release by querying how busy their neighbours are. The number of congested neighbours a node can have is

$$\zeta = \sum_{v \in \mathcal{G}} \theta(n_v(t)) \tag{58}$$

where $\mathcal{G}$ is the set containing the neighbours of node, $n_v(t)$ is the number of packets in node v at time t and θ is the Heaviside function $\theta(x > 0) = 1$ and $\theta(x \leq 0) = 0$.

It is shown in [58] that simple traffic rules can self-organize the traffic network centred on a definite mean rate $\lambda_c < \lambda >$. Then $\lambda_c =< N > / < T >$ where $N(t) = \sum_{s_i \in V} q(s_i, t)$, where $q(s_i, t)$ is the queue length at node s_i at time t. Thus $N(t)$ is the total queue length over all vertices V of the network. The time T is averaged over all successfully released/delivered packets. If ζ is the number of congested neighbours, the packet injection rate $\lambda_i(t)$ for host i is updated as follows:

$$\lambda_i(t+1) = \begin{cases} \min\{1, \lambda_i(t) + \mu\}, & \zeta < 4 \\ 0 & \zeta \geq 4. \end{cases} \tag{59}$$

The general principle of transmission control protocol of conservative increase and rapid decrease is adopted here. In fact the transmission drops to zero when all neighbouring nodes are congested.

If the neighbouring nodes are not congested the load increases at a rate of μ, and drops to zero if all the neighbours are congested. This control mechanism is inspired by the "additive increase/multiplicative decrease" [54] used in packet networks. Valverde and Solé studied this

control method in a Manhattan network with *Poisson* traffic and unlimited queue capacity. It was noticed that the packet release and the density of hosts satisfies the relation $\lambda \sim \rho^{-1}$ (see Eq. 33). On average, the packet release reaches a steady critical state. This does not mean that the local traffic creation rates are all similar, as the congestion levels vary widely between nodes. An interesting observation made by Valverde and Solé is the existence of a synchronization effect in the congestion state of distinct nodes.

The mean field model for a homogeneous network with average node degree $< k >$ and and finite variance $< k^2 >$. The time evolution of packet density is $\Gamma(t) = N(t)/M$ in the limit of infinite queue is defined by

$$\frac{d\Gamma}{dt} = \rho\lambda - \frac{< k >}{D}\Gamma(1 - \Gamma), \tag{60}$$

where D is the network diameter, and T is the average transient time.

The system has two equilibrium points $\Gamma_{\pm} = 1 \pm (1 - 4\rho\lambda D/ \langle k \rangle^{\frac{1}{2}})/2$ for $\lambda > \lambda_c \equiv < k > /4D\rho$. For $\lambda >< k > /4D\rho$, the fixed points vanish and no finite density exists. In this "congested phase", the density of packets grows without bounds. For $\lambda < \lambda_c$, a finite stable density Γ_- is observable (the other fixed point Γ_+ is unstable). For the unstable case [24] we recover $\lambda_c = 2/L$ for packet traffic on a square lattice of size $L \times L$. For this network the average length of the route is $D = L/2$. If there is a feedback mechanism between the load λ, some other finite Γ^* will be achieved. In the equilibrium situation, the scaling relation will be observed, i.e. $\lambda \sim \rho^{-1}$ between the packet release rate and the density of hosts. The mean field field calculation assumed a fixed load λ was being used. The previous rules actually introduce self-regulation of traffic injection rates at the hosts. In other words, if the traffic level N defines an order parameter, it will interact with a control parameter (λ), reducing it when N is large and increasing it when N is low. The mean field equations can be extended assuming finite H to become

$$\frac{d\Gamma}{dt} = \rho\lambda(1 - \frac{\gamma}{H}) - \frac{< k > \Gamma}{D};\ \frac{d\lambda}{dt} = \mu(1 - \lambda) - \frac{\Gamma}{< k >} \tag{61}$$

For low density levels ($\Gamma << H$). The system has a single a symbolically stable fixed point. Numerical simulations of this model on a Poissonian graph agree with these predicted values. Topological input is given only in terms of averaged values, and does not display the homgeneous architecture assumed by Poissonian graphs, [21].

7.3 Real routing policies

Actual routing tables do not send packets at random. An element of efficiency is involved, with respect to minimum distance or latency. There are likely to be local aberations to this overall objective. Real routing protocols reflect this with different *levels* of routing rules. There are *infra-* and *inter-* autonomous systems. Intra is prevalently shortest path, and inter-AS routing does not follow any minimization criteria (and could indeed be random). So a parameter that

can be introduced is the local sphere of nodes within m-hops of a given vertex that would define the 'infra' zone, see [59] and also for an excellent overview in Valverde's thesis [56].

7.4 Control in scale-free networks using *TCP*

The above model is an oversimplified packet network as the topology of a real network is, of course, not a regular network. Also, the model does not allow for packets dropped in transit (as occurs in the Internet) because of the unlimited queues on the nodes. In this section we introduce a more realistic model by considering a scale-free network generated using the *IG* algorithm with a power law decay index of 2.22. Similarly to the previous simulations, each node is designated as either a host or a router. Routers have a single routing queue that receives packets in transit across the network, and releases them back onto the network at a rate governed by the connectivity of the node. The difference with the previous examples is that for this network the simulation is of the fixed-increment time advance type rather than next-event time advance. This allows the routing queue service rate to be set as Ck^{α}, C constant packets per time tick of the simulation, where k is the degree of the router node. This means that nodes with larger degrees produce more traffic. The index α has been chosen to be between 1 and 2 here. Hosts have identical routing queues and function in the same way, but additionally act as sources. They have transmit buffers that hold packets generated by *LRD* and Poisson traffic sources until they have been acknowledged. The exact mechanism for this is described below.
The control mechanism uses a simplified version of *TCP* Reno [54] as the network protocol. This is the predominate protocol used on the Internet at present. This version is derived from that described in Erramilli *et al* [18]. It concentrates on the slow-start mechanism because in real networks this not only affects all connections, but is also the dominant effect for most connections. It also has a more marked effect on the network dynamics than congestion avoidance.
As in our previous sections, a double intermittency map is used as the basis for each *LRD* traffic source, and a uniform random number generator for each Poisson source. However, they are used in a slightly different way. One sojourn period in the '*on*' side represents a whole file which is then *windowed* using the *TCP* slow start algorithm: at the start of the file the window size is set to 1. Only a single packet is sent at that time tick. When a packet reaches its destination an acknowledgement is returned to the source: once this packet has been acknowledged, the window size is doubled and the next two packets are sent. When both these packets have been acknowledged, the window size is doubled again and a new window of packets is sent. The doubling process is repeated until the end of the file or the maximum window size (a fixed value). This is described mathematically in section 3.3 on *TCP* dynamics.
The routing algorithm uses a pre-calculated look-up table of shortest paths. All links between nodes are assumed to have unit length. At each time step packets are forwarded from the head of each routing queue. If an acknowledgement packet reaches its destination, this triggers the release of the next window of packets from that host.
In Fig. 19 we see comparisons are made between the different topologies and packet transport

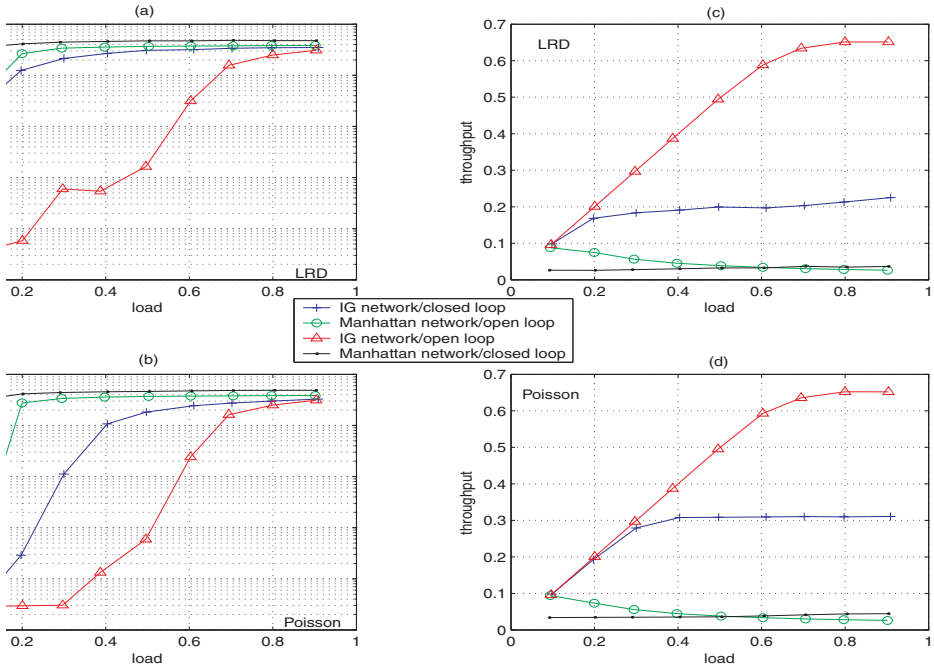

Figure 19: Comparisons between the open-loop simulations and closed-loop simulations on regular networks and scale-free *IG* networks. Network sizes and host densities are the same for all simulations.

algorithms used in this and the previous work [65]. Four combinations for networks are considered:

- scale-free(produced using the *IG* model) with a closed-loop algorithm (*TCP*).
- Manhattan with an open-loop algorithm.
- scale-free(produced using the *IG* model) with an open-loop algorithm.
- Manhattan network with a closed-loop algorithm.

The network has 1024 nodes and the host density is taken to be 589/1024 for all cases. The index α of the server strength $0.25n^{\alpha}$ is fixed at 1 for all four combinations. The host distribution is random for the Manhattan network; the *IG* network connectivity 1 and 2 nodes are selected to be hosts. This is closer to a random distribution and the difference it makes is seen in Fig. 19. In Fig. 18(a) average lifetimes are shown as a function of the load for the four cases with *LRD* traffic sources at each host. Average lifetimes include the waiting time in transmit buffers and measurements from actual networks would not include this. Also, loads quoted are those offered to the transmit buffers, rather than the loads exiting these buffers which enables end users experience to be modelled.
Clearly the closed-loop *TCP* algorithm increases lifetimes for both regular and scale free networks. The requirement of *TCP* that packets be acknowledged before the next window of packets

is sent is restrictive in the sense that new windows cannot be sent by hosts more frequently than the round trip times (RTT) or ping times. Congestion is reacted to immediately because it causes an increase in RTT's and makes sources back off. Since file sizes are not that great and window sizes are often reset to 1 due to the round-trip time maximum RTO limit, throughput can never be that high. This results in packets being delayed in the transmit buffer and is the primary cause of increased packet lifetimes. By contrast the open-loop algorithm does not react to congestion and allows unlimited queues to build up at routers. For sufficiently high loads open-loop networks become congested and lifetimes approach those of the closed-loop networks.
In addition, Fig. 19(a) shows that the network topology is also a very important factor. In fact, a Manhattan network with an open-loop algorithm has longer lifetimes than an *IG* network with a closed-loop algorithm primarily because of the much shorter average path lengths in the *IG* network. The average path length in the Manhattan network is 16 'hops' (one 'hop' is the distance between neighbouring nodes). By contrast in an *IG* network ordinary nodes connect to rich nodes with a high probability, and rich nodes also connect to one another preferentially. This leads to much shorter average path lengths.
In Fig. 19(b) the same measurements are made with Poisson traffic sources substituted for *LRD* sources. Results are very similar.
Fig. 19(c) shows throughput plotted against load. Results are consistent with those for average lifetime. Identical networks using open-loop algorithms have higher throughputs; the *IG* network performs more efficiently for both types of algorithm. Similar behaviour is observed for Poisson sources.
Thus, regular open-loop simulations are fundamentally different to the closed-loop simulations of *IG* networks and so detailed comparisons are not very useful.
Fig. 20 shows a comparison of different server strengths. Two types of source are considered. The same *IG* network with the same pattern of hosts is used. Results from *LRD* sources and Poisson sources differ greatly. Throughputs (Figs 19(c) and 19(d)) at the lower server strengths (α equal to 1 and 1.1) are qualitatively similar: the throughput matches the load up to a threshold and then levels out. However, this threshold is more than 50% higher for the Poisson sources. If the exponent α is increased to a value of 1.5 this threshold can no longer be seen; throughputs for the two source types are similar. When servers are strongest ($\alpha = 2.0$) the situation is reversed: the network with *LRD* sources has a higher throughput, able to handle the maximum load applied to it without becoming overloaded.
In Fig. 21 3D plots show transmit and routing queue lengths for the same network. Again both types of traffic source were used. The server strength, α, is only 1 here. Nodes are arranged in ascending order of connectivity. In Figs 21(a) and (b) transmit queue lengths are linked to the average lifetimes for both types of source. At low loads they are very short; as loads increase they rise in length rapidly.
The routing queues (Figs 21 (c) and (d)) are much shorter. There is no pattern to the queue lengths for *LRD* sources, with the exception that all queues arise at the higher connectivity

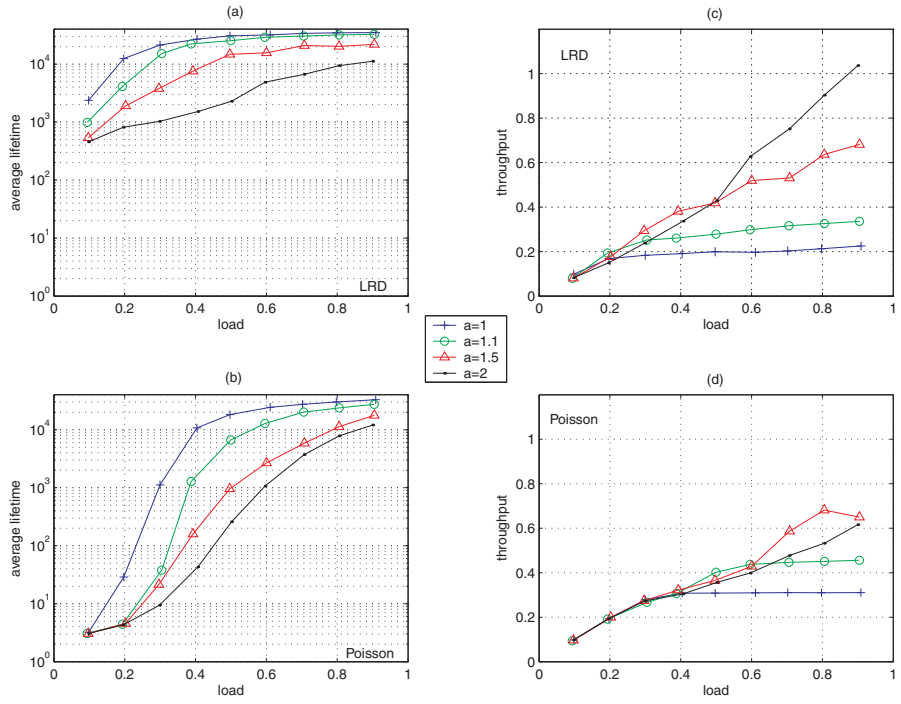

Figure 20: The number of packets that can be served at each time instant is increased according to a power law n^{α}, where n is the degree of the node and $\alpha = 1, 1.1, 1.5, 2$.

nodes. Poisson sources produce different behaviour. Queue lengths are much less but still increase with increasing load. In addition the same nodes have queues at different loads. This implies that host distribution is important. The highest connectivity nodes build up queues for all loads. As might be expected these nodes are the most congested. At higher server strengths connectivity becomes less significant as would be expected.

The fact that much longer queues form in the transmit buffers shows that these queues provide the main contribution to average lifetimes.

In Fig. 22 we have simulated the packet dropping of real networks by limiting the routing queue lengths. The same network and host pattern as described for Fig. 19 has been used with a server strength $\alpha = 1$. Very severe packet loss has been modelled here in order to test the extreme situation. Real networks generally suffer much less packet loss.

For *LRD* sources (Fig. 22(a)) average lifetimes are greatly reduced when the queue limit is decreased. When queue lengths are limited, packets are dropped at the routers and therefore re-sent more frequently. This causes shorter waits in the transmit buffer. This can be seen most clearly at the very low queue length limit.

In the case of Poisson sources (Fig. 22(b)) average lifetimes behave quite differently. Lifetimes peak at a load of 0.3 for the queue limit of 5. This peak shifts to higher values as the queue limit increases. When there is no queue limit the lifetimes are the same in regular networks.

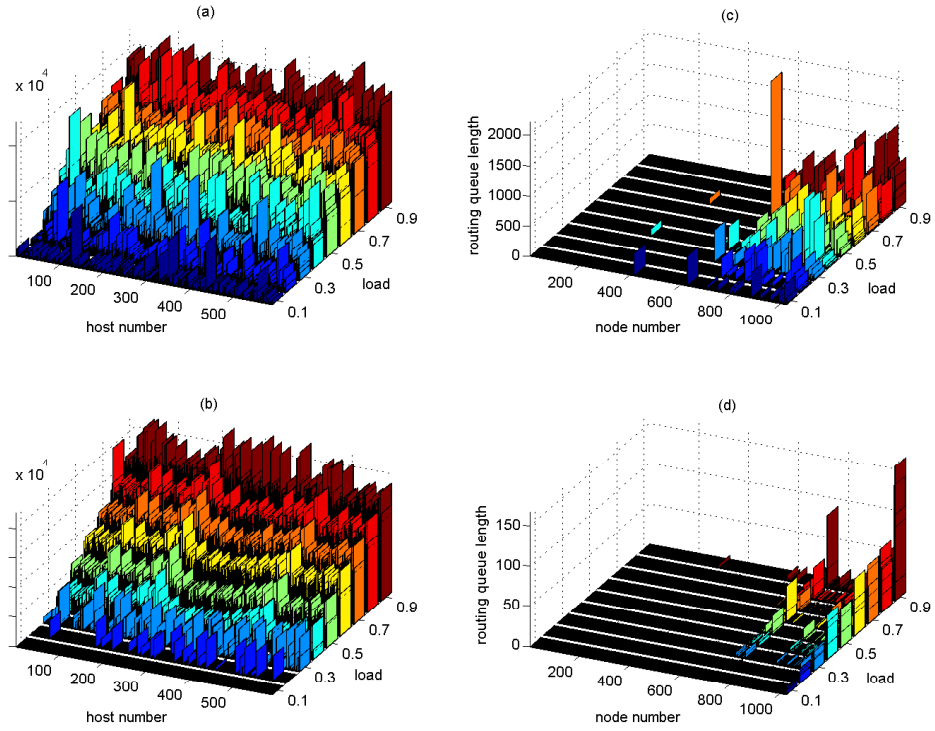

Figure 21: Queue lengths for host nodes of an *IG* network are shown as load increases, for both Poisson and *LRD* sources.

Fig. 22(c) shows throughputs for *LRD* sources. These are greatly reduced when a queue limit is applied. At the smaller queue limits throughput is close to zero. In the case of Poisson sources (Fig. 22(d)) throughput is similar for the queue limit of 100, but also much less at the lower queue limits. However, throughputs are still much higher than for the *LRD* sources. This is caused by the shorter queues in the case of Poisson sources. Most queue lengths are less than a 100, meaning that this limit has little effect.

If the same *IG* network is used, but hosts are selected randomly with the same density of 589/1024 then results are similar to those presented in Fig. 23. The network with randomly placed hosts always performs slightly better than the one with hosts placed at the low degree hosts. Average lifetimes are lower and throughput slightly higher. This apparently shows that the inclusion of a small number of rich nodes in fact makes little difference.

8 Topologically changing network performance

This work is based on the paper [14]. The essence of the traffic modelling is to make comparisons so that robust indicators of important characteristics can be indentified. An example of how we can do this is to use a model of network generation that allows a transition between different classes of networks. Here we illustrate the idea with a transition from random to scale-free networks. The transition allows us to consider three different topological types of networks: (a)

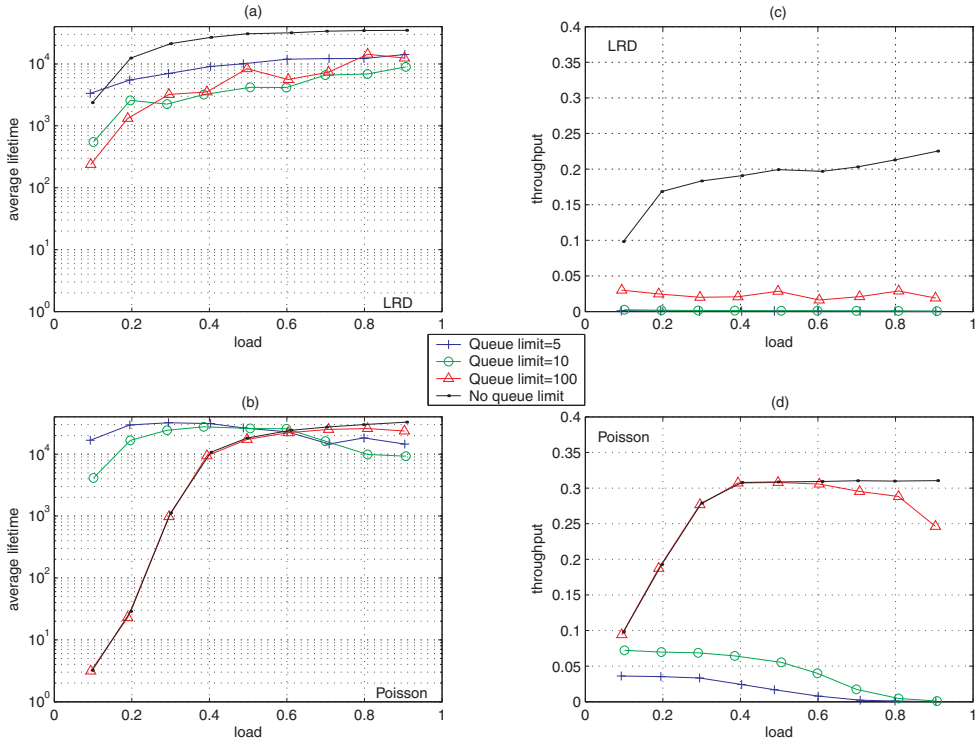

Figure 22: Effect of varying queue length limit on average packet life time and throughput for *LRD* and Poisson sources.

random; (b) scale-free with $\gamma = 3$; (c) scale-free with $\gamma = 2$. We also use an LRD traffic generator in order to reproduce the fractal behavior that is observed in real world data communication.
We also allow the queue length restrictions and transmission rates to reflect the importance of the node in the network in terms of the the node degree. We show that these two factors can induce drastic changes in the throughput and delivery time of network performance and are able to counter-balance some undesirable effects due to the topology.
We consider the class of networks generated by the model introduced in [33]. This model is particularly interesting since it allows a parameterized transition between random (homogenous) and scale-free (heterogenous) graphs. In particular, scale-free graphs are characterized by the presence of few very high degree vertices, called *hubs*, which are responsible for a drastic reduction of the average distance between network nodes.
In [15], we have already studied the effects of such a transition on the network communication performance. The main result shows that, somewhat surprisingly, the structure of scale-free graphs, which are ubiquitous in nature, does not lead to any benefit but rather a worsening in terms of the end-to-end performance. In particular, the characteristic parameters known as *throughput* and *delivery time* were considerably affected by the congestion at the network hubs. This is counter-intuitive when one considers that the shortening of the distances in the network might result in a reduction of the delivery time and thus an increase of the throughput.

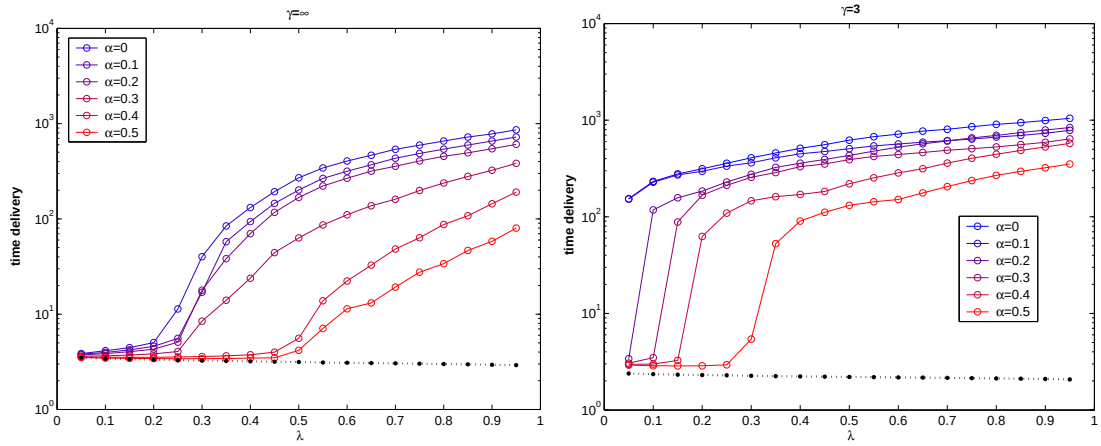

Figure 23: Delivery time versus the generation rate, λ. The network is a (a) random graph ($\gamma = \infty$), (b) scale-free graph ($\gamma = 3$) with number of nodes $N = 512$ and number of edges $M = 2N$. We show the effects of varying the transmission rates $r(i)$ at node i, according to the law $r(i) = k(i)^{\alpha}$, for α ranging between 0 and 0.5 (blue to red). The black dotted line represents the free regime at $\alpha = 1$.

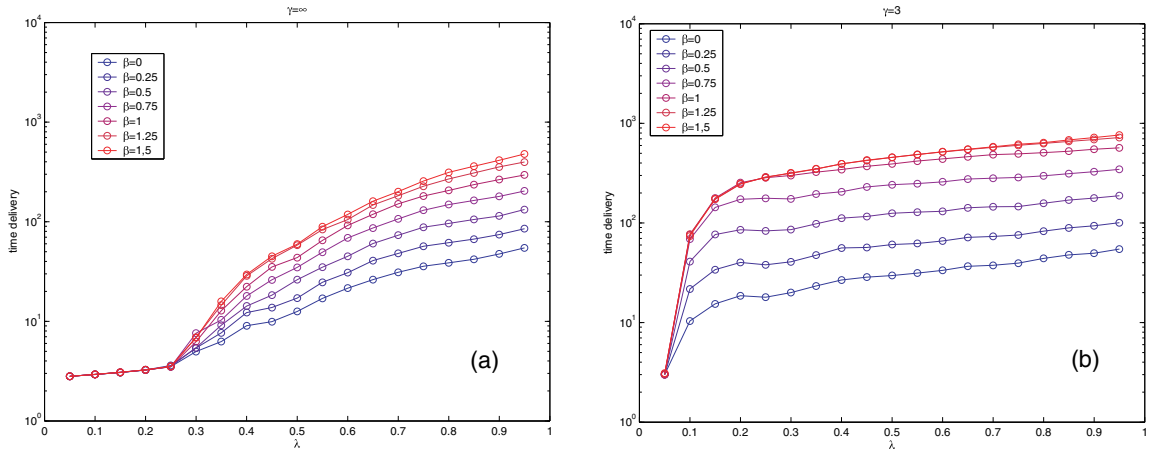

Figure 24: Delivery time versus the generation rate, λ. The network is a (a) random graph ($\gamma = \infty$), (b) scale-free graph ($\gamma = 3$) with number of nodes $N = 512$ and number of edges $M = 2N$. We show the effects of varying the queue length $q(i)$ at node i, according to the law $q(i) = 50k(i)^{\beta}$, for β ranging between 0 and 1.5 (blue to red).

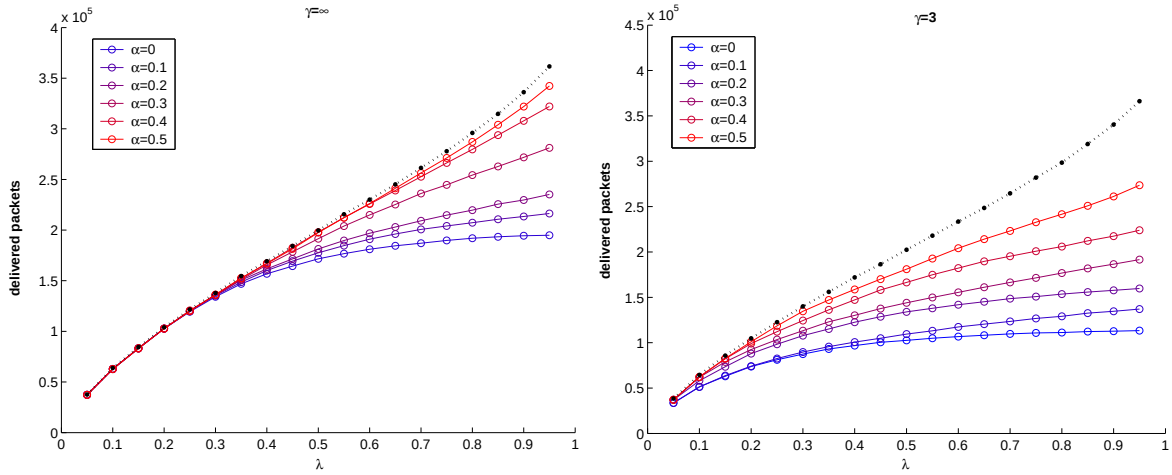

Figure 25: Number of delivered packets versus the generation rate, λ. The network is a (a) random graph ($\gamma = \infty$), (b) scale-free graph ($\gamma = 3$) with number of nodes $N = 512$ and number of edges $M = 2N$. We show the effects of varying the transmission rates $r(i)$ at node i, according to the law $r(i) = k(i)^{\alpha}$, for α ranging between 0 and 0.5 (blue to red). The black dotted line represents the free regime at $\alpha = 1$.

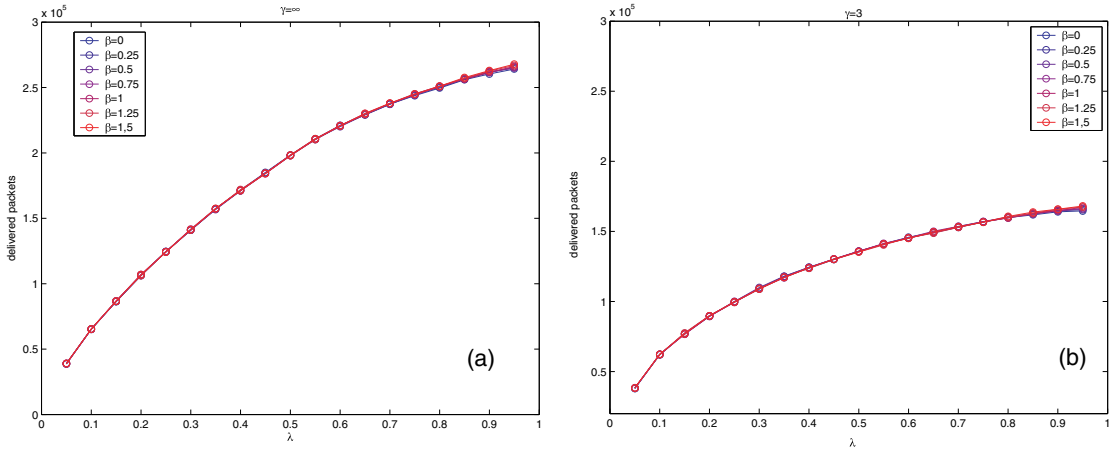

Figure 26: Number of delivered packets versus the generation rate, λ. The network is a (a) random graph ($\gamma = \infty$), (b) scale-free graph ($\gamma = 3$) with number of nodes $N = 512$ and number of edges $M = 2N$. We show the effects of varying the queue length $q(i)$ at node i, according to the law $q(i) = 50k(i)^{\beta}$, for β ranging between 0 and 1.5 (blue to red).

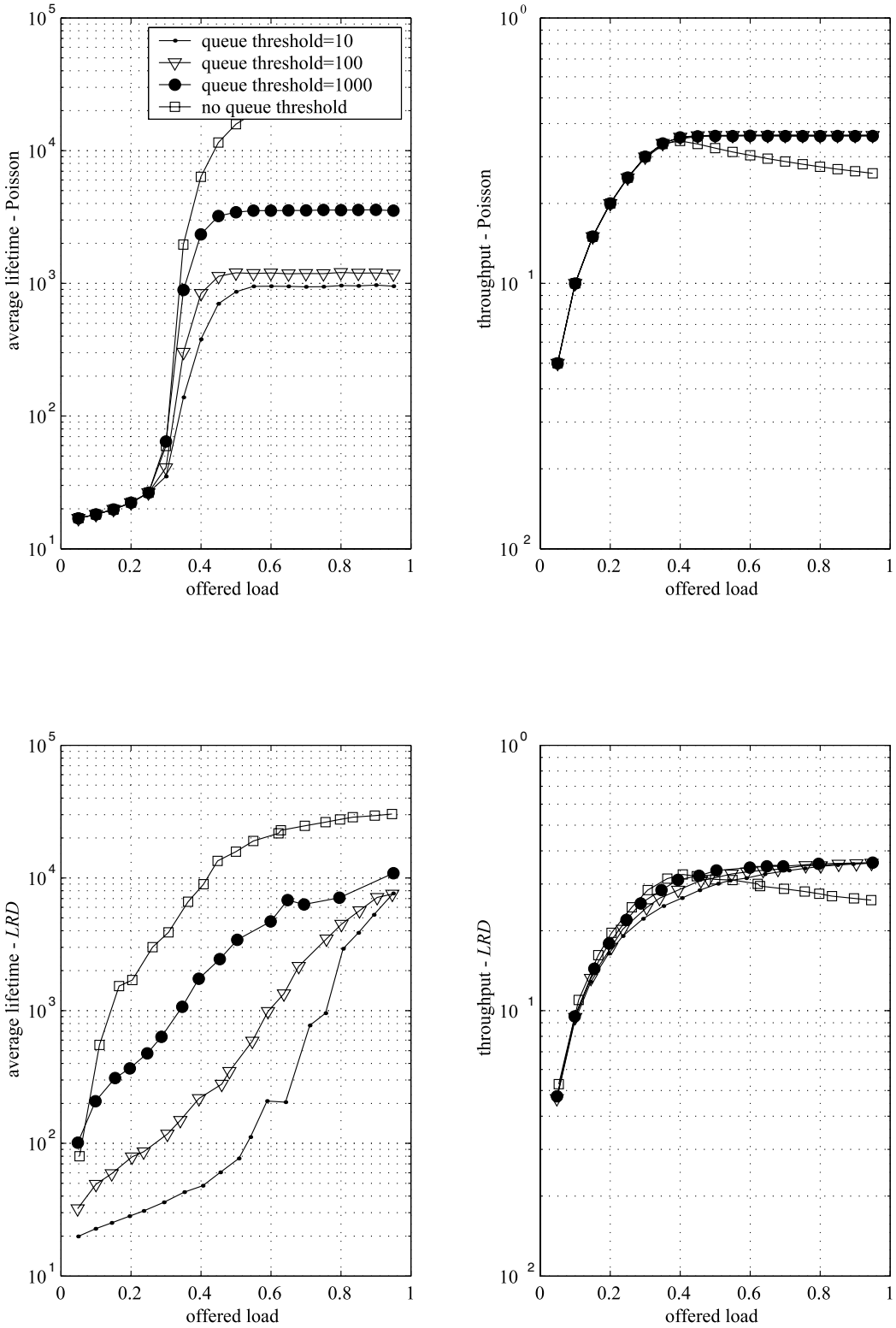

Figure 27: Number of dropped packets versus the generation rate, λ. The considered network is scale-free with $\gamma = 3$ and $\gamma = \infty$, the number of nodes being $N = 512$ and number of edges $M = 2N$. We show the effects of varying the queue length $q(i)$ at node i, according to the law $q(i) = 50k(i)^{\beta}$, for β ranging between 0 and 1.5.

This interesting phenomenon is analogous to the *paradox of heterogeneity* [1], which has been observed in the context of the synchronization of scale-free networks. Indeed, it is unrealistic to assume that resources such as bandwidth are uniformly distributed among the network nodes in strongly heterogenous networks. Instead, it is very likely that hubs, which are characterized by a high number of incoming and outgoing links, are found to play a fundamental role in communication over the network. They are typically characterized by having higher server strength transmission rates and larger buffers than more peripheral nodes in the network. Here we consider the following variation to the study presented in [15]:

- The transmission rate r is assumed to scale with the degree at each vertex i, $k(i)$, as: $r(i) = c_1 k(i)^\alpha$ (note that in the particular case where $\alpha = 0$, we recover the original case, with all the nodes having the same transmission rates);
- the maximum queue length (i.e., the buffer size) is no longer assumed infinite but is taken to scale with the degree at each vertex i, $k(i)$, as: $q(i) = c_2 k(i)^\beta$.

We use the power laws above not necessarily for accurate simulation of the nature of distributed transmission rates and buffer sizes, but for their qualitative properties which emphasizes the importance of these hubs. In what follows, we analyze separately, by means of numerical simulations, the effects of varying α and β on the network communication performance. As a representative case, we assume $c_1 = 1$ and $c_2 = 50$. Similar behaviour was observed for other values of c_1 and c_2.

Then we compare the behaviors of networks characterized by different topological features. More precisely, networks will be considered with different degree distributions; the degree k at a given node being the number of incident links at the node. Particular emphasis will be given to scale-free topologies in which the degree distribution is observed to follow a power law, i.e. $P(k) \sim k^{-\gamma}$ [2, 42, 36, 16].

In order to produce the transition from random to scale-free network we use the static model introduced in [33]. Vertices are indexed by an integer i, for $(i = 1...., N)$, and assigned a *weight* or *fitness* $p_i = i^{-\eta}$ where η is a parameter between 0 and 1. Two different vertices are selected with probabilities equal to the normalized weights, $p_i / \sum_k p_k$ and $p_j / \sum_k p_k$, and an edge is added between them unless one exists already. This process is repeated until M edges are made in the system leading to the mean degree $\langle k \rangle = 2M/N$. This results in the expected degree at vertex i scaling as $k_i \sim (\frac{N}{i})^\eta$ [33]. We then have the degree distribution, i.e. the probability of a vertex being of degree k, given by $P(k) \sim k^{-\gamma}$ with $\gamma = 1 + \frac{1}{\eta}$. Thus, by varying η, we can obtain the exponent γ in the range, $2 < \gamma < \infty$. Moreover the ER graph is generated by taking $\eta = 0$.

It is worth noting that the static model described here can be considered as an extension of the standard ER model for generating *random* scale-free networks, i.e. networks with prescribed degree distribution, but completely random with respect to all the other features.

The set-up is as before for a host and router network with the host density set at $\rho = 0.16$. The shortest distance route algorithm is used with the proviso that if a choice of link is available, the shortest queue node wins.

Packets enter the queue from one side (the *end*) and leave it from the other one (the *head*). The head of the queue contains a variable number of packets equal to the transmission rate at the node. The queue at each node i, has a finite maximum length, $q(i)$. If the packets arriving at the queue at vertex i result in the number of packets exceeding $q(i)$, then the excess packets are dropped.

Using the network model in this section and traffic generator detailed above, simulations were carried out to analyse various aspects of end-to-end performance for two types of network. Namely, results for random graphs have been paired with those of scale-free graphs with $\gamma = 3$. We have calculated the corresponding output for scale-free graphs with $\gamma = 2$ and have found that the differences in behavior with the alternative value $\gamma = 3$ are negligible by comparison with the behavior of the random graph, and so the third set of comparisons is not repeated here. In Fig. 23 we see that random graphs respond more quickly with smaller delivery times as α increases (from zero). Fig. 24 shows that the communication is much more efficient in terms of delivered packets at high loads (or generation rate) as α increases. Moreover, as shown in Fig. 25 (where the effects of variable transmission rates have been highlighted), scale-free networks behave worse than random graphs for a sufficiently high value of the parameter α (of the order of unity, from our simulations). The number of delivered packets, shown in Fig. 26, instead, is observed to be unaffected by the buffer sizes at the nodes, being mainly determined by the network topology. Finally, in Fig. 27, the number of dropped packets is observed to decrease as the buffer sizes are scaled more sensitively with vertex degree.

These graphs show up several features of a representative model of communication networks contrasting the network performance when the graph considered is random or scale-free. The results show that there is no obvious benefit for communication networks having scale-free growth patterns across all performance indicators.

References

[1] C. Zhou A.E. Motter and J.Kurths. *Phys.Rev.E*, 71, 2005.

[2] A.L.Barabasi and R.Albert. *Science*, 286, 1999.

[3] R. Albert, H. Jeong, and A. Barabási. Error and attack tolerance of complex networks. *Nature*, 406:378–381, 2000.

[4] R. H. Albert, A. Jeong, and A.-L. Barabási. Diameter of the world wide web. *Nature*, 401:130–131, 1999.

[5] D.K. Arrowsmith, R.J. Mondragon, J.M.Pitts, and M. Woolf. Internet packet traffic congestion. *Nonlinear Dynamics for Coding Theory and Network Traffic, in the IEEE Proceedings of Systems and Circuits*, 3:746–749, 2003.

[6] D.K. Arrowsmith, R.J. Mondragón, J.M. Pitts, and M.Woolf. Phase transitions in packet traffic on regular networks: a comparison of source types and topologies,. *Preprint*, 2004.

[7] D.K. Arrowsmith and M.Woolf. Modelling of TCP packet traffic in a large interactive growth network. *IEEE Proceedings of Systems and Circuits*, 5:477–480, 2004.

[8] A. L. Barabási and R. Albert. Emergence of scaling in random networks. *Science*, 266:509–512, 1999.

[9] M. Barenco and D.K. Arrowsmith. The autocorrelation of double intermittency maps and the simulation of computer packet traffic. *Jnl of Dynamical Systems*, 19(1):61–74, 2004.

[10] J. Beran. Statistics of long memory processes,. *Monographs on Stats and Appl. Prob.*, 61, 1994. Chapman & Hall.

[11] B. Bollobás. Degree sequences of random graphs. *Discrete Maths.*, 33:1–19, 1981.

[12] B. Bollobás. *Random Graphs.* Academic Press, 1985.

[13] R. Cohen and S.Havlin. Scale–free Networks are Ultrasmall. *Phys. Rev. Lett.*, 90(5):058701, 2003.

[14] F. Sorrentino D.K. Arrowsmith, M. di Bernardo. Communication models with distributed transmission rates and buffere sizes. *ISCAS'06 Proc.*, 2006.

[15] M. di Bernardo D.K. Arrowsmith and F.Sorrentino. Effects of variation of load distribution on network performance.

[16] S.N. Dorogovtsev and J.F.F. Mendes. *Evolution of Networks.* Oxford University Press, New York, 2003.

[17] P. Erdös and A. Rényi. On Random Graphs I. *Publ. Math. Debrecen*, 6:290–297, 1959.

[18] A. Erramilli, M. Roughan, D. Veitch, and W. Willinger. Self-similar traffic and network dynamics. *Proc. of the IEEE*, 90(5):800–819, May 2002.

[19] A. Erramilli, R. P. Singh, and P. Pruthi. Chaotic Maps as Models of Packet Traffic. *In Proc. ITC 14, The Fundamental Role of Teletraffic in the Evolution of Telecommunication Networks*, pages 329–338, 1994.

[20] A. Erramilli, R. P. Singh, and P. Pruthi. An application of deterministic chaotic maps to model packet traffic. *Queueing Systems*, 20:171–206, 1995.

[21] M. Faloutsos, P. Faloutsos, and C. Faloutsos. On Power-Law Relationships of the Internet Topology. *Proc. ACM/SIGCOMM, Comput. Commun. Rev.*, 29:251–262, 1999.

[22] H. H. Fowler and W. Leland. Local Area Network Traffic Characteristics, with Implications for Broadband Network Congestion Management. *IEEE Jour. on Sel. Areas in Comm*, 9:1139–1149, September 1991.

[23] L.C. Freeman. A set of measures of Centrality based on Betweeness. *Sociometry*, 40:35–41, 1977.

[24] H. Fukś and A. T. Lawniczak. Performance of data networks with random links. *Mathematics and Computers in Simulation*, 51:103–119, 1999.

[25] H. Fukś, A.T. Lawniczak, and S. Volkov. Packet delay in data network models. *ACM Transactions on Modeling and Computer Simulation*, 11(3), 2001.

[26] K. Fukuda, H. Takayasu, and M. Takayasu. Origin of critical behavior in Ethernet traffic. *Physica A*, pages 289–301, 2000.

[27] A. Giovanardi, G. Mazzini, and R. Rovatti. Chaos based self–similar traffic generators. *Proc. NOLTA*, pages 747–750, 2000.

[28] K. I. Goh, E. Oh, K. Kahng, and D. Kim. Betweenness centrality correlation in social networks. *Phys. Rev. E*, 67:017101, 2003.

[29] P. Holme and B. J. Kim. Vertex Overload Breakdown in Evolving Networks. *Physical Review E*, 65:066109, 2002.

[30] C. Huang, M. Devetsikiotis, I. Lambadaris, and R. Kaye. Fast Simulation for Self-Similar Traffic in ATM Networks. In *Gateway to Globalization, 1995 IEEE International Conference on Communications*, volume 1, pages 438–444, Seattle, Washington, 1995. IEEE ICC95.

[31] B. E. Huberman and R. M. Lukose. Social dilemmas and Internet congestion. *Science*, 277:535–537, 1997.

[32] R. Jain and S. A. Routhier. Packet trains: Measurements and a new model for computer network traffic. *IEEE Journal on Selected Areas*, 4:986–995, 1986.

[33] B. Kahng K.-I. Goh and D.Kim. Universal behavior of load distribution in scale-free networks. *Phys.Rev.Lett.*, 2001.

[34] L. Kleinrock. *Queueing Systems. v. 1. Theory.* John Wiley & Sons, 1975.

[35] L. Kocarev and G. Vattay. *Complex dynamics in communication networks.* Springer Verlag, Berlin, Germany, 2005.

[36] M.Berthlemy L.A.N. Amaral, A. Scala and H.E.Stanley. *Proc.Natl.Acad.Sci.USA*, 97, 2000.

[37] W. E. Leland, M. S. Taqqu, W. Willinger, and D. Wilson. On the Self-Similar Nature of Ethernet Traffic (Extended Version). *IEEE/ACM Trans on Networking*, 2, No 1(1):1–15, Feb. 1994.

[38] H. Li and M. Maresca. Polymorphic-torus network. *IEEE Transs Comp.*, 38(9):1345–1351, 1989.

[39] B. Mandelbrot. Self-Similar Error Clusters in Communication Systems and the Concept of Conditional Stationarity. *IEEE Trans. On Communication Technology*, COM-13:71–90, March 1965.

[40] B. Mandelbrot and J.W. Van Ness. Fractional Brownian Motions, Fractional Noises and Applications. *SIAM Review*, Vol. 10, No 4:422–437, October 1968.

[41] J. L. McCauley. *Chaos, Dynamics and Fractals and Algorithmic Approach to Deterministic Chaos*. Cambridge University Press, 1995.

[42] P.Faloutsos M.Faloutsos and C.Faloutsos. *Comput.Commun.Rev.*, 29.

[43] R. J. Mondragón. A Model of Packet Traffic using a Random Wall Model. *Int. Jou. of Bif. and Chaos*, 9 (7):1381–1392, 1999.

[44] R. J. Mondragón. Congestion and centrality. *in preparation*, 2004.

[45] I. Norros. Studies on a model for connectionless traffic, based on fractional brownian motion. *Conf. On Applied Probability in Engineering, Computer and Communication Sciences*, Paris:16–18, June 1993.

[46] T. Ohira and R. Sawatari. Phase Transition in Computer Network Traffic Model. *Physical Review E*, 58:193–195, 1998.

[47] Y. Pomeau and P. Maneville. Intermittent transition to turbulence in dissipative dynamical systems. *Commun. Math. Phys.*, 74:189–197, 1980.

[48] P. Pruthi. *An application of chaotic maps to packet traffic modelling*. PhD thesis, KTH, Stockholm, Sweden, Oct. 1995.

[49] P. Pruthi and A. Erramilli. Heavy-Tailed ON/OFF Source Behaviour and Self-Similar Traffic. *ICC 95*, June 1995.

[50] M. Roughan and D. Veitch. A Study of the Daily Variation in the similarity of Real Data Traffic. *Tech. Rep. 0070, SERC, Software Engineering Research Centre, Level 3, 110 Victoria St, Carlton Vic, 3053, Australia*, 1997.

[51] H. Schuster. *Deterministic Chaos: An introduction*. Wiley-VCH, 1995.

[52] R. V. Solé and S. Valverde. Information transfer and phase transitions in a model of internet traffic. *Physica A*, 289:595–605, 2001.

[53] W. Stallings. *Data and Communications*. Prentice Hall Int. Inc., 2000.

[54] W. R. Stevens. *TCP/IP Illlustrated*, volume Volume 1: The Protocols. Addison-Wesley, 1994.

[55] L. Subramanian, S. Agarwal, J. Rexford, and R. H. Katz. Characterizing the Internet Hierarchy from Multiple Vantage Points. *Proc. of INFOCOM 2002*, June, 2002.

[56] S. Valverde. *Evolution and Dynamics in Information Networks.* http://complex.upf.es/ sergi/theis$_s$*valverde.pdf*, $DepartamentdeFisícaAplicada, UniversitatPolytèc$

[57] S. Valverde and R.V. Solé. Self-organized critical traffic in parallel computer networks. *Physica A*, 312:636, 2002.

[58] S. Valverde and R.V. Solé. Self-organized critical traffic in parallel computer networks. *Physica A*, 312:636–653, 2002.

[59] S. Valverde and R.V. Solé. Internet's critical path horizon. *Eur. Phys. Jnl B*, 38:245–252, 2004.

[60] D. Veitch. Novel Models of Broadband Traffic. In *Proc. Globecom '93*, pages 362–368, Murray River, Australia, 1992. 7th Australian Teletraffic Research Seminar.

[61] X-J Wang. Statistical physics of temporal intermittency. *Phys Rev A*, 40(11):664761, 1989.

[62] W. Willinger, M. S. Taqqu, R. Sherman, and D. V. Wilson. Self-similarity through high-variability: statistical analysis of Ethernet LAN traffic at the source level. *IEEE/ACM Transactions on Networking*, 5(1):71–86, 1997.

[63] R.J. Wilson. *Introduction to Graph Theory*. Longman Group Limited, Whistable Kent, Great Britain, 1972. ISBN:0-582-44762-3.

[64] J. Winick and S. Jamin. Inet–3.0 Internet Topology Generator. *Tech. Report UM-CSE-TR-456-02, University of Michigan*, 2002.

[65] M. Woolf, D.K. Arrowsmith, R.J. Mondragón, and J. M. Pitts. Optimization and phase transition in a chaotic model of data traffic. *Physics Reviews E*, 66:056106, 2002.

[66] M. Woolf, D.K. Arrowsmith, S. Zhou, R.J.Mondragón, and J.M. Pitts. Dynamical modelling of *tcp* packet traffic on scale-free networks. *Proc of Mittag-Leffler Inst.*, 2004.

[67] S. Zhou and R. J. Mondragón. Towards Modelling the Internet Topology – The Interactive Growth model. In *Proc. of ITC18*, 2003.

[68] S. Zhou and R. J. Mondragón. Accurately modelling the internet topology. *submitted to Physical Review E*, 2004.

[69] S. Zhou and R. J. Mondragón. Redundancy and robustness of the *as*-level internet topology and its models. *IEE Electronic Letters*, 40(2):151–152, January 2004.